Multiproduct Characterization of Surface Soil Moisture Drydowns in the United Kingdom

Chak-Hau Michael Tso,[a] Eleanor Blyth,[b] Maliko Tanguy,[b] Peter E. Levy,[c] Emma L. Robinson,[b] Victoria Bell,[b] Yuanyuan Zha,[d] and Matthew Fry[b]

[a] U.K. Centre for Ecology and Hydrology, Lancaster, United Kingdom
[b] U.K. Centre for Ecology and Hydrology, Wallingford, United Kingdom
[c] U.K. Centre for Ecology and Hydrology, Edinburgh, United Kingdom
[d] State Key Laboratory of Water Resources and Hydropower Engineering Science, Wuhan University, Wuhan, China

ABSTRACT: The persistence or memory of soil moisture (θ) after rainfall has substantial environmental implications. Much work has been done to study soil moisture drydown for in situ and satellite data separately. In this work, we present a comparison of drydown characteristics across multiple U.K. soil moisture products, including satellite-merged (i.e., TCM), in situ (i.e., COSMOS-UK), hydrological model [i.e., Grid-to-Grid (G2G)], statistical model [i.e., Soil Moisture U.K. (SMUK)], and land surface model (LSM) [i.e., Climate Hydrology and Ecology research Support System (CHESS)] data. The drydown decay time scale (τ) for all gridded products is computed at an unprecedented resolution of 1–2 km, a scale relevant to weather and climate models. While their range of τ differs (except SMUK and CHESS are similar) due to differences such as sensing depths, their spatial patterns are correlated to land cover and soil types. We further analyze the occurrence of drydown events at COSMOS-UK sites. We show that soil moisture drydown regimes exhibit strong seasonal dependencies, whereby the soil dries out quicker in summer than winter. These seasonal dependencies are important to consider during model benchmarking and evaluation. We show that fitted τ based on COSMOS and LSM are well correlated, with a bias of lower τ for COSMOS. Our findings contribute to a growing body of literature to characterize τ, with the aim of developing a method to systematically validate model soil moisture products at a range of scales.

SIGNIFICANCE STATEMENT: While important for many aspects of the environment, the evaluation of modeled soil moisture has remained incredibly challenging. Sensors work at different space and time scales to the models, the definitions of soil moisture vary between applications, and the soil moisture itself is subject to the soil properties while the impact of the soil moisture on evaporation or river flow is more dependent on its variation in time and space than its absolute value. What we need is a method that allows us to compare the important features of soil moisture rather than its value. In this study, we choose to study drydown as a way to capture and compare the behavior of different soil moisture data products.

---

1. Introduction

While accounting for 0.001% of Earth's water by volume (Oki et al. 2004), soil moisture (θ) is a primary environmental variable controlling many hydrological and ecological processes. It plays a critical role in crop yield and plant growth (de Wit and van Diepen 2008), hillslope stability (Talebi et al. 2007), ecosystem function (D'Odorico et al. 2003), and human health (Bomblies and Eltahir 2009). Perhaps more significantly, however, it is its overall control of land surface water and energy balance coupling and land–atmosphere feedback that make

it so critical to understand soil moisture dynamics. Resting at the interface between land and air, soil moisture affects evapotranspiration and serves as the link between global water and energy cycles (Akbar et al. 2018b; Fatichi et al. 2016) in a changing climate (Seneviratne et al. 2010) and exerts control on near-surface air temperature (Schwingshackl et al. 2017), which impacts the development and persistence of droughts (Turner et al. 2021), floods (Bonan and Stillwell-Soller 1998; Rong et al. 2022; Wasko et al. 2022), heatwaves (Lorenz et al. 2010), and wildfires (Krueger et al. 2015). It has also been shown from both process models and observations that soil moisture (especially water table depth) exerts an effect of the atmospheric boundary layer (Maxwell et al. 2007; Dirmeyer et al. 2014). Projections have shown that decreased soil moisture will lead to future positive trends in potential evapotranspiration (PE) due to soil moisture feedbacks on the atmosphere (Berg et al. 2016), which can exacerbate future drought conditions (Zhou et al. 2019). Finally, an increasing body of evidence shows soil moisture and its feedback to atmosphere controls soil carbon uptake (e.g., Humphrey et al. 2021; Kerr and Ochsner 2020; Green et al. 2019).

⓪ Denotes content that is immediately available upon publication as open access.

🖉 Supplemental information related to this paper is available at the Journals Online website: https://doi.org/10.1175/JHM-D-23-0018.s1.

Corresponding author: Chak-Hau Michael Tso, mtso@ceh.ac.uk

Soil moisture values govern evapotranspiration regimes (Haghighi et al. 2018; Seneviratne et al. 2010). Specifically, extended drying in the absence of rainfall can cause soil moisture to fall below a threshold value—leading to a transition from energy- to water-limited evapotranspiration regimes. Under water-limited regimes, evapotranspiration is no longer limited by the amount of energy available, but is instead limited by the amount of moisture present. As a result, evapotranspiration is reduced with decreasing soil moisture, which results in an increase in sensible heating of the lower atmosphere (Berg et al. 2014; Seneviratne et al. 2010), thus providing an important control on surface meteorological conditions.

There exist many different soil moisture observations and estimates. Traditionally, ground-based measurements are used to monitor soil moisture. For example, time-domain reflectometry (TDR; e.g., Robinson et al. 2003) and time domain transmissometry (TDT; e.g., Blonquist et al. 2005) probes are used to measure moisture content indirectly based on the correlation to electric and dielectric properties of materials, while neutron probes are used to measure soil moisture based on neutron scattering. These probes tend to only capture information local to the probe and require manual measurements at a site—thus, they are not suitable for long-term monitoring that represents a larger area and a depth profile. Geophysical surveys, such as ground penetrating radar (GPR) or electrical resistivity tomography (ERT), can also be used to monitor soil moisture at site scale and at depths of tens of meters (e.g., Tso et al. 2019; Dafflon et al. 2009; Beff et al. 2013). Their main advantage is that they can provide a geophysical image that describes the spatial pattern of soil moisture and they have recently been used to image and monitor root water uptake. Finally, cosmic ray neutron (COSMOS) probes are commonly used nowadays for ground-based soil moisture measurements. It can measure soil moisture at a relatively large footprint (typically top 15–83 cm of soil over the horizontal radius footprint ranging from 130 to 240 m depending on air humidity, soil moisture, and vegetation; Köhli et al. 2015) and it can take measurements continuously and at near–real time (Zreda et al. 2012). Over the past 10 years, the number of COSMOS monitoring stations have grown globally (i.e., >100 stations and mobile platforms). COSMOS measurements have also been investigated for their information content on soil hydraulic properties (Brunetti et al. 2019).

While ground-based measurements can only provide soil information at point locations around the globe, passive and active microwave satellite missions/sensors (SMAP, SMOS, ASCAT, AMRS-2, Sentinel-1, and other legacy missions) as well as optical instruments (e.g., MODIS, Sentinel-2, and others) provides excellent coverage, originally at coarse resolution (25–50 km) but making rapid progress toward high-resolution mapping (i.e., 0.1–1 km) (Peng et al. 2021a), including many efforts of downscaling (Abbaszadeh et al. 2019; Long et al. 2019). Recently, a 6-hourly, 30-m soil moisture over the conterminous United States (CONUS), SMAP-HydroBlocks, has become available between 2015 and 2019 (Vergopolan et al. 2021, 2022, 2020). Satellite soil moisture measurements are typically thought to be capturing soil moisture information up to the top few centimeters of the land surface (Akbar et al. 2018a). A recent paper, however, argues L-band (1.4 GHz) measurements can sense at least 3–5 times deeper than commonly thought (Feldman et al. 2023).

There are also satellite products that combine data from multiple satellites. The European Space Agency (ESA) CCI SM product (Dorigo et al. 2017) combines various single-sensor active and passive microwave soil moisture products into three harmonized products: a merged ACTIVE, a merged PASSIVE, and a COMBINED active and passive microwave product, with the current version providing data from 1978 to present. For a complete review of ground, proximal, and satellite remote sensing of soil moisture, see Babaeian et al. (2019).

The third way to estimate soil moisture is the use of models, which has the advantage of being continuous in time and space. Process models that represent the laws of physics can be used in this regard. Land surface models (LSMs; e.g., JULES, Noah-MP, ORCHIDEE) (e.g., Blyth et al. 2021) capture the dynamics of water mass and energy balance by representing various land surface processes, including plant interactions with land and atmosphere. LSMs usually take a whole-system approach to model the land surface and they output a large number of variables, such as total evapotranspiration and components, runoff, surface temperature, soil temperature, snow mass, latent and sensible heat, net and gross primary productivities, in addition to soil moisture. Hydrological models of different formulations (Meng and Quiring 2008) are also useful to produce continuous estimates of soil moisture. They calculate the mass balance in the different components of the water cycle and prescribe hydraulic parameters to simulate their behavior. For example, it has been used recently to study extremes and wetting and drying dates under future climate conditions (Kay et al. 2022). In contrast to process models, data-driven models, including statistical and machine learning models, cast soil moisture as a response variable and seeks to describe it as a function of a number of predictor variables (e.g., Ghosh et al. 2014). Commonly used predictor variables include precipitation, temperature land use, and other proxies of site conditions. These models do not require specification of physically based model parameters, boundary conditions, or domain discretization. Rather, relationships are derived between the response and predictor variables.

There exist many global soil moisture data products. For example, "SoMo.ml" (O and Orth 2021) is trained using a long short-term memory (LTSM) machine learning model based on in situ data collected from more than 1000 stations and provides multilayer soil moisture data (0–10, 10–30, and 30–50 cm) at 0.25° spatial and daily temporal resolution over the period 2000–19. Topography, GLDAS (Rodell et al. 2004) static variables, and ERA5 daily meteorological forcing data were used to train the model. Wang et al. (2021) developed seven global, gap-free, long-term (1970–2016), multilayer (0–10, 10–30, 30–50, and 50–100 cm) θ products at monthly 0.5° resolution by synthesizing a wide range of θ datasets using three statistical methods (unweighted averaging, optimal linear combination, and emergent constraint). Finally, a key challenge has been the use of high-quality in situ data to improve low resolution/accuracy of satellite data (e.g., Tomer et al. 2016). A novel LTSM deep learning model (Liu et al. 2022) has been developed to combine

the multiscale data to predict 9-km daily soil moisture (5-cm depth) over CONUS.

All of these products available are being used to inform important aspects of the environment such as weather forecasting, drought, agriculture, and landslide risk. However, the array of products and the different scales horizontally, vertically, and in time that they represent means that evaluating models can be very challenging. One thing that they all have in common is that they all respond in the same way to the atmosphere: they wet up when it rains and dry out when rain stops. This key aspect of the land surface is critical to all of those applications, namely, how quickly the land dries after a rainfall event. While there has been a prolonged interest in studying soil moisture memory persistence, particularly its relation to root zone, the availability of global and national datasets from satellite, sensor networks, and gridded models have led to intensive characterization of soil moisture drydown in recent years, especially the characteristic drydown decay time scale (τ; days) or the e-folding time of the process. Shellito et al. (2016) was the first to report SMAP soil moisture drying more rapidly than observed in situ following rainfall events. Martínez-de la Torre et al. (2019b) studied the drydown processes of global hydrological models (Water-GAP, SWBM) and LSMs (JULES, HTESSEL, ORCHIDEE, SURFEX) and flux tower evapotranspiration data and show that LSMs are in agreement with general patterns. They show much higher τ than satellites because ET from models and flux tower data has access to deeper soils. McColl et al. (2017) and Sehgal et al. (2021a) both provides a global analysis of satellite soil moisture drydown, with the former showing τ is lower in regions with sandier soils, and in regions that are more arid. Akbar et al. (2018a) classifies the CONUS into ET regimes based on satellite θ drying rates, while Dong et al. (2022) repeat the same with flux tower, surface (5 cm) and vertically integrated (0–50 cm) in situ observations. Specifically, two regimes are defined: water-limited (soil moisture is a limiting factor for ET) and energy-limited (ET is insensitive to soil moisture for adequately wet conditions, and is primarily determined by atmospheric evaporative demands). Sehgal et al. (2021a) characterize the global soil moisture drydown pattern from SMAP satellite data at 36 km resolution by plotting the distribution of the canonical form of the surface soil moisture loss function. They show strong seasonal variability of drydown parameters, especially in the grasslands, croplands, and savannah landscapes. High values of falling rate loss in stage-II ET (i.e., equivalent to low τ) is observed for the arid and semiarid regions, especially for the seasons when the atmospheric moisture demand is high. Soil texture exerts influence on the drydown parameters when the soil moisture is low. Sehgal et al. (2021b) further develops indices such as relative rate of drydown and flash drought stress index from satellite data for global flash drought monitoring. Soil moisture drydown can also be used to improve the parameterization of land surface models. For example, Raoult et al. (2021) have evaluated and optimized in the ORCHIDEE LSM using data assimilation. They found that the decay parameter τ does not appear correlated to soil type, consistent with Martínez-de la Torre et al. (2019b) but not with McColl et al. (2017). Ruscica et al. (2020)

considered drydowns from a couple of satellite products and the ORCHIDEE LSM for a large region in southeastern South America and highlighted the importance of sampling frequency and observational errors in τ estimates.

What remains lacking is a comprehensive comparison of the various soil moisture products and their drydown characteristics. Many studies have compared soil moisture estimates from satellite, modeled, and in situ soil moisture data products (Beck et al. 2021; Deng et al. 2020). However, to our knowledge, there has not been a comparison of drydown characteristics from these different types of data products. We focus on drydown as it is important for most applications such as evaporation modeling, feedbacks into the atmosphere, runoff generation and agriculture. It is also possible to measure and model it at a range of scales and therefore a range of observations can be used to benchmark the models. This method avoids the pitfalls of comparing actual soil moisture, which is subject to soil properties and which is less important for the end result of modeling the role of soil moisture in the environment.

Using both rainfall- and soil moisture–based drydown identification techniques, we compare the drydown events and τ values at COSMOS-UK sites for different products available for the United Kingdom, as well as present median τ maps at 1–2 km resolution for the different gridded products. Specifically, we seek to answer the following research questions: (i) how consistent or different are the τ maps of different gridded products, (ii) what are the key factors controlling their spatial and temporal patterns of τ, and (iii) if the lack of rainfall is used to select common drydown events at sites, how correlated are the τ values obtained from the different products? We describe the datasets and methods in section 2, present results in section 3, and provide discussions and conclusions for this study in sections 4 and 5.

2. Datasets and methods

We compare the performance of multiple soil moisture data products in the United Kingdom from the period 2016–18. We consider daily data and all gridded data have a spatial resolution of 1 or 2 km. When comparing gridded datasets to data at COSMOS-UK stations, the grid cell which a COSMOS-UK station is located within is matched to that station.

a. Data products

1) POINT DATA AND DATA PRODUCTS

(i) COSMOS-UK

The Cosmic-ray Soil Moisture Observing System (COSMOS) measures soil moisture (θ) based on the theory that the neutrons derived from cosmic rays are attenuated by water present in soil. Volumetric soil moisture is derived from corrected neutron counts based on site-specific field calibration (H. M. Cooper et al. 2021; Evans et al. 2016; Franz et al. 2013). COSMOS-UK (https://cosmos.ceh.ac.uk) (H. M. Cooper et al. 2021; Evans et al. 2016) is a long-term network of moisture monitoring sites in the United Kingdom equipped with cosmic-ray neutron probes (Zreda et al. 2012) and is part of the COSMOS-EUROPE
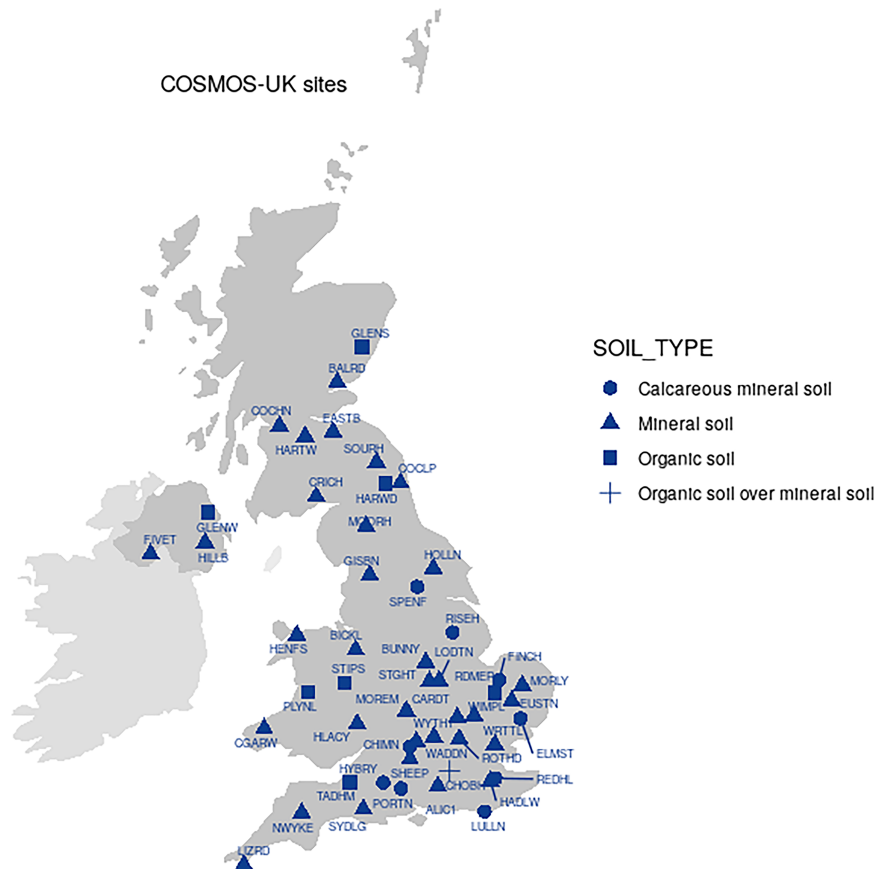
Fig. 1. Map of COSMOS-UK sites and their HOST soil type.

network (Bogena et al. 2022). The network's 51 sites cover a wide range of land cover, rainfall, elevations, and soil type. COSMOS-UK dataset has been frequently used for soil moisture assessment and data assimilation (e.g., E. Cooper et al. 2021), as well as comparison with other soil moisture data products (e.g., Peng et al. 2021b). Figure 1 and Table 1 show a map and summary of the COSMOS-UK network, respectively.

(ii) TDT probes

At many of the COSMOS-UK sites, at least two TDT soil moisture sensors are installed at various depths to provide absolute volumetric water content and soil temperature for the validation of COSMOS data. TDT is similar to TDR, but it measures the transmission, rather than reflection, of a pulse along a looped, or closed circuit, rod. TDT measures the time taken for an electromagnetic wave to propagate (travel) along a given length of a transmission line in the soil, which allows an estimate of the dielectric constant of the medium. In this paper, TDT1 and TDT2 are buried at 0.1-m depth and are located 1 m apart from each other.

2) GRIDDED DATA PRODUCTS

Four daily gridded U.K. soil moisture datasets is considered. A summary of the products is given in Table 2.

(i) Grid-to-Grid

The Grid-to-Grid (G2G) model is a fully distributed grid-based hydrological (runoff production and routing) model which uses spatial datasets to represent spatial heterogeneity in the landscape (Bell et al. 2009). Surface and subsurface runoff from each 1-km grid box provide the lateral inflows to the routing scheme. Although G2G was originally developed to estimate river flows at a national scale, here, the focus is its soil water storage component.

The G2G model requires gridded time series of precipitation, potential evapotranspiration (PE), and temperature (T) as input driving data. In the G2G model output considered in this work, they are:

- Daily 1-km grids of precipitation [CEH Gridded Estimates of Areal Rainfall (CEH-GEAR)] (Keller et al. 2015; Tanguy et al. 2021), divided equally over each model time step within a day.
- Monthly 40-km grids of short grass PE [Meteorological Office Rainfall and Evaporation Calculation System (MORECS)] (Hough and Jones 1997), retrieving the 1-km grid and extended where necessary by duplicating from the nearest 1-km box with data, then divided equally over each model time step within a month.
- Daily 1-km grids of min and max T (HadUK-Grid) (Met Office et al. 2022), interpolated through the day using a sine curve (Bell et al. 2016).

TABLE 1. List of COSMOS-UK sites used in the current study. RDMER is no longer operational since 20 Sep 2018 but this does not affect our analysis.

Station name	Station ID	Elevation (m)	Land cover	Start date
Alice Holt	ALIC1	80	Deciduous broadleaf forest	6 Mar 15
Balruddery	BALRD	130	Farmland	16 May 14
Bickley Hall	BICKL	78	Improved grassland	28 Jan 15
Bunny Park	BUNNY	39	Arable	27 Jan 15
Cardington	CARDT	29	Grassland	24 Jun 15
Chimney Meadows	CHIMN	65	Grassland	2 Oct 13
Chobham Common	CHOBH	47	Heath	24 Feb 15
Cockle Park	COCLP	87	Grassland and arable	21 Nov 14
Crichton	CRICH	42	Grassland	2 Dec 14
Easter Bush	EASTB	208	Grassland	14 Aug 14
Elmsett	ELMST	76	Arable	11 Aug 16
Euston	EUSTN	18	Improved grassland	31 Mar 16
Gisburn Forest	GISBN	246	Coniferous woodland	15 Aug 14
Glensaugh	GLENS	399	Grass and heather moorland	14 May 14
Hadlow	HADLW	33	Improved grassland	27 Oct 16
Hartwood Home	HARTW	225	Grassland/woodland	20 May 14
Harwood Forest	HARWD	300	Coniferous woodland	20 May 15
Henfaes Farm	HENFS	287	Semi-natural grassland	17 Dec 15
Hollin Hill	HOLLN	82	Grassland	25 Mar 14
The Lizard	LIZRD	85	Grassland/heath	17 Oct 14
Loddington	LODTN	186	Arable	26 Apr 16
Lullington Heath	LULLN	119	Grassland/heath	16 Dec 14
Moor House	MOORH	565	Cotton grass/heather	4 Dec 14
Morley	MORLY	55	Arable	14 May 14
North Wyke	NWYKE	181	Grassland/pasture	16 Oct 14
Plynlimon	PLYNL	542	Semi-natural grassland	5 Nov 14
Porton Down	PORTN	146	Grassland	18 Dec 14
Redmere	RDMER	3	Shallow arable	11 Feb 15
Redhill	REDHL	91	Improved grassland	18 Feb 16
Riseholme	RISEH	53	Improved grassland	4 May 16
Rothamsted	ROTHD	131	Crops and grassland	25 Jul 14
Sheepdrove	SHEEP	170	Grassland	24 Oct 13
Sourhope	SOURH	487	Coarse grassland	9 Dec 14
Spen Farm	SPENF	57	Arable and horticulture	23 Nov 16
Stoughton	STGHT	130	Arable	18 Aug 15
Stiperstones	STIPS	432	Heathland	6 Nov 14
Tadham Moor	TADHM	7	Grassland	14 Oct 14
Waddesdon	WADDN	98	Grassland	4 Nov 13

In G2G, total water storage in the soil column (water volume per unit area) is conceptualized as "available" and "residual" water storages, where the residual water is held under tension forces and is not available for drainage but can contribute to evaporation. Specifically, the available (WS), maximum available (WS$_{max}$), and residual (WS$_r$) water storages in the soil column are given by

$$WS = L(\theta - \theta_r)$$
$$WS_{max} = L(\theta_{sat} - \theta_r)$$
$$WS_r = L\theta_r, \quad (1)$$

where θ, θ_s, and θ_r are the total, saturation, and residual water contents (water volume per unit volume of soil, $0 \le \theta \le 1$) and L is soil depth. Thus, $\theta = (WS + WS_r)/L$. The soil field capacity θ_{fc} is assumed to be dependent on the saturation water content θ_s via $\theta_s = 1.25\theta_{fc}$. A derived quantity called the Hydrology of Soil Types (HOST) class (Boorman et al. 1995) has been used

to infer estimates of soil hydraulic properties across the United Kingdom; values of θ_{fc}, θ_r, and L have been statistically associated with each of the 29 HOST classes using soil properties extracted from the SEISMIC database (Hallett et al. 1995). Note that G2G considers the entire soil column present and different HOST classes are associated with different depths to groundwater (i.e., soil depths, see Fig. S2 in the online supplemental material for map). G2G has also been widely used for flood risk and high and low river flows (Bell et al. 2016; Kay et al. 2021a; Lane and Kay 2021). The G2G is generally used to estimate natural river flows, but recent work has shown that including datasets of observed abstractions and discharges can improve G2G simulation of gauged river flows (Rameshwaran et al. 2022).

(ii) Soil moisture U.K.

Soil moisture U.K. (SMUK; Levy and COSMOS-UK Team 2023) is a parsimonious statistical model built to represent the

TABLE 2. Summary of different gridded soil moisture data products considered in this study. All products have a daily resolution.

Product	Period considered	Sensing depths and spatial resolution	Forcing data, dependencies, notes
SMUK	23 Mar 2016 to 31 Dec 2018 (daily)	Comparable to that of COSMOS 2-km resolution	Statistical model Forcing data: Met Office NIMROD and NWP-UKV Currently conditioned on COSMOS observations
G2G	1 Jan 2017 to 31 Dec 2018 (daily)	Depth of the soil column (a few centimeters to several meters) 1-km resolution	Gridded hydrological model Forcing data: CEH-GEAR, MORECS, HadUKGrid
CHESS	1 Jan 2016 to 31 Dec 2017 (daily)	Fixed layers of depths [0–10 cm], [10–35 cm], [35–100 cm], and [100–300 cm] (can be converted to COSMOS sensing depths) 1-km resolution	CHESS-land output from the JULES land surface model Forcing data: CHESS-met, Land Cover Map 2000
TCM	1 Jan 2016 to 31 Dec 2017 (daily)	Few centimeters 1-km resolution	This is a merge of two satellite products (ASCAT and SMAP) and CHESS

spatiotemporal variation of U.K. soil moisture. After evaluation of several options, the final form of the fitted function is

$$\theta_{ts} = \theta_{\min} + \beta_1 \langle P \rangle_{ts} + \beta_2 T_{ts} + \beta_3 I_{SW,ts} + \beta_4 C_s, \quad (2)$$

where T_{ts} is the air temperature at time t and location s; $I_{SW,ts}$ is the scatterometer synthetic aperture radar (SCAT-SAR) satellite-based soil water index (Bauer-Marschallinger et al. 2018); C_s is the organic carbon at location s from the Countryside Survey (CS; Henrys et al. 2012); and β_1, β_2, β_3, and β_4 are regression coefficients. Exponential moving average (EMA) $\langle P \rangle$ of the rainfall time series P instead of P itself is used to handle the nonlinear dependence of soil moisture to the history of rainfall in the preceding days (i.e., noninstantaneous rainfall). The EMA rainfall at time t is calculated as

$$\langle P \rangle_t = \langle P \rangle_t \times k + \langle P \rangle_{t-1} \times (1 - k), \quad (3)$$

where $k = 2/(n + 1)$, n is the number of time points in the moving averaged window, and the angled brackets denote the EMA filter. In the SMUK data considered in this work, the 2-km rainfall dataset used is taken from the Met Office NIMROD system (Met Office 2003), which uses processed radar and satellite data, together with surface reports and numerical weather prediction (NWP) fields. Similarly, air temperature input data are taken from Met Office U.K. Atmospheric High Resolution Model data (NWP-UKV) (Met Office 2016).

A Hamiltonian Markov chain Monte Carlo procedure is used to calibrate the parameters in Eq. (2). Starting with uninformative priors, the model parameters are estimated using data from CS sites. Using the posterior distribution of this step as priors, posterior parameter distributions are estimated using soil moisture data from COSMOS-UK. Finally, the fitted model is applied to a 2-km grid across the United Kingdom to estimate posterior distribution of θ for each day.

b. CHESS

The Joint U.K. Land Environment Simulator (JULES) is a community land surface model (LSM) designed to be used as a standalone LSM driven by observed forcing data, or coupled to an atmospheric global circulation model (Best et al. 2011). Water and energy balance at the land surface are considered and soil moisture is controlled by the interplay of infiltration, soil type and hydraulic characteristics, and root zone dynamics. The soil hydrology component of JULES is based on a finite difference approximation to the Richards' equation (Zha et al. 2019; Richards 1931). The JULES model used a fixed vegetation map based on observations in Land Cover Map 2000 (Fuller et al. 2002) to prescribe the land cover fractions of the 8 different categories: broad leaf trees, needle leaf trees, grass, crops, shrub, water, bare soil, and urban.

Soil moisture is a key LSM variable and various efforts has been made to improve the representation of soil moisture in JULES (E. Cooper et al. 2021; Pinnington et al. 2021; Martínez-de la Torre et al. 2019a). The JULES soil moisture data product considered in this work is the water, carbon and energy fluxes simulation for Great Britain using the JULES Land Surface Model and the Climate Hydrology and Ecology research Support System meteorology dataset (CHESS-land) (Martinez-de la Torre et al. 2018; Blyth et al. 2019), which uses a standardized, gridded daily meteorological forcing dataset at 1-km resolution (CHESS-met) (Robinson et al. 2020a, 2017) as input.

JULES gives soil moisture estimates at various depths; in standard configuration these correspond to four layers, with depths [0–10 cm], [10–35 cm], [35–100 cm], and [100–300 cm]. The JULES layers are often referred to by their thicknesses, which are 10, 25, 65, and 200 cm, respectively. We refer to these four layers as $CHESS_{10}$, $CHESS_{25}$, $CHESS_{65}$, and $CHESS_{200}$ hereafter. The COSMOS metadata provides the D_{86} values, which represent the empirically determined

effective depths where 86% of the interactions between cosmic rays and water molecules occur (Köhli et al. 2015). For each day, we calculate a depth-adjusted JULES soil moisture estimate, $\theta_{CHESS_{adj}}$, depending on the D_{86} value provided for that day, such that

where $D_{86} \leq 10$ cm, $\theta_{CHESS_{adj}} = \theta_{CHESS_{10}}$,

where 10 cm $< D_{86} \leq 35$ cm,

$$\theta_{CHESS_{adj}} = \left(\frac{10}{D_{86}} \times \theta_{CHESS_{10}}\right) + \left(\frac{D_{86} - 10}{D_{86}} \times \theta_{CHESS_{25}}\right),$$

where 35 cm $< D_{86} \leq 100$ cm,

$$\theta_{CHESS_{adj}} = \left(\frac{10}{D_{86}} \times \theta_{CHESS_{10}}\right) + \left(\frac{25}{D_{86}} \times \theta_{CHESS_{25}}\right)$$
$$+ \left(\frac{D_{86} - 35}{D_{86}} \times \theta_{CHESS_{65}}\right), \qquad (4)$$

where θ_{10}, θ_{25}, and θ_{65} are the JULES predicted soil moisture values from the [0–10 cm], [10–35 cm], and [35–100 cm] layers, respectively, and the D_{86} value is given in cm. In this way, thickness-weighted contributions to the soil moisture are taken from every JULES layer which would be wholly or partly contained within the D_{86}. We will focus on individual CHESS layers, particularly the top 10 cm ($CHESS_{10}$). For site-based comparison with COSMOS data, we will focus on the CHESS outputs adjusted to COSMOS depths (D_{86}) (i.e., $\theta_{CHESS_{adj}}$).

We also use PE data from CHESS-PE (Robinson et al. 2020b) for calculating excess soil moisture (ESM). Similar to the definition of excess rainfall (i.e., rainfall available for direct runoff, which is the total amount of rainfall minus all abstractions including interception, depression storage, and infiltration), ESM is defined as soil moisture available that exceeds PE, which is equivalent to

$$ESM = (\theta \Delta z - PE \Delta t), \qquad (5)$$

where ESM is in millimeters and Δz is the thickness of the soil column considered in millimeters. PE is in millimeters per day and is multiplied by the duration Δt of 1 day so that ESM evaluated at the daily time scale. Negative ESM is possible when $PE \Delta t > \theta \Delta z$.

TRIPLE COLLOCATION MERGED (TCM)

TCM is a merged data product created by merging three gridded soil moisture products—two from satellite (ASCAT and SMAP) and one from LSM (CHESS-land)—using triple collocation (Peng et al. 2021b; Tanguy et al. 2022). The Advanced Scatterometer (ASCAT), on board the EUMETSAT's *MetOp-A*, *MetOp-B*, and *MetOp-C* satellites provides backscatter measurements (active microwave observations) that are used to derive surface soil moisture, represented by degree of saturation (Wagner et al. 2013). The Soil Moisture Active Passive (SMAP) satellite (Entekhabi et al. 2010) is a NASA mission to monitor global land surface soil moisture and freeze/thaw state. Different levels of soil moisture products have been developed and published. For deriving the TCM product, the SMAP L3E

product (enhanced level 3, https://nsidc.org/data/SPL3SMP_E/versions/3) at 9-km resolution based on passive radiometer measurements was used. Triple collocation error estimation (Gruber et al. 2017; Chen et al. 2018) in combination with least squares merging scheme is used to merge the three datasets by treating them as independent to each other, which in turn allows weighted averaging of the products in a way that takes into account the error characteristics of the individual datasets (Peng et al. 2021b). The original data output is at 12.5-km resolution in order to match with the resolution of ASCAT. A 1-km resolution version has been produced by downscaling the three individual products to 1 km before merging.

c. Evaluation of time series similarity at COSMOS sites

Three statistical metrics that have been widely adopted in the soil moisture community (e.g., Gruber et al. 2020), namely, Pearson correlation coefficient (R), unbiased root-mean-square error (ubRMSE), and the Lin's concordance correlation coefficient (Lin 1989) are used to quantify the differences between two soil moisture products. These metrics are defined as follows:

$$R = \frac{\text{cov}(\theta_{Product1}, \theta_{Product2})}{\sqrt{\text{var}(\theta_{Product1})}\sqrt{\text{var}(\theta_{Product2})}}, \qquad (6)$$

$$\text{ubRMSE} = \sqrt{\left[(\theta_{Product1} - \overline{\theta_{Product1}}) - (\theta_{Product2} - \overline{\theta_{Product2}})\right]^2}. \qquad (7)$$

The overbar here denotes the mean, while var(·) and cov(·) denote the variance and covariance, respectively. The Lin's concordance correlation coefficient (LCC) is defined as

$$\text{LCC} = \frac{2R(\theta_{Product1}, \theta_{Product2})\sqrt{\text{var}(\theta_{Product1})}\sqrt{\text{var}(\theta_{Product2})}}{\text{var}(\theta_{Product1}) + \text{var}(\theta_{Product2}) + (\overline{\theta_{Product1}} - \overline{\theta_{Product2}})^2}. \qquad (8)$$

d. Evaluation of drydown

FITTING DRYDOWN CURVES

Following previous work (Rondinelli et al. 2015; McColl et al. 2017; Shellito et al. 2016; Kurc and Small 2004), we fit a drydown curve in the form of

$$\theta = a\exp\left(-\frac{t}{\tau}\right) + \theta_{wp}, \qquad (9)$$

where θ is the volumetric moisture content (m^3 m^{-3}), t is the elapsed time in days, a is a fitting constant (which represents the absolute change in θ in the fitted drydown sequence), τ is the characteristic drydown in days, and θ_{wp} is the empirical wilting point or asymptotic minimum θ at the end of the drydown sequence. An illustration of the curve fitting routine is provided in Fig. 2. It is also noteworthy that $1/\tau$ is equivalent to the slope of $-d\theta_{decreasing}$ versus θ in stage-II drydown for evapotranspiration (ET, using τ as a proxy for ET loss) or drainage loss (e.g., Akbar et al. 2018b; McColl et al. 2017).
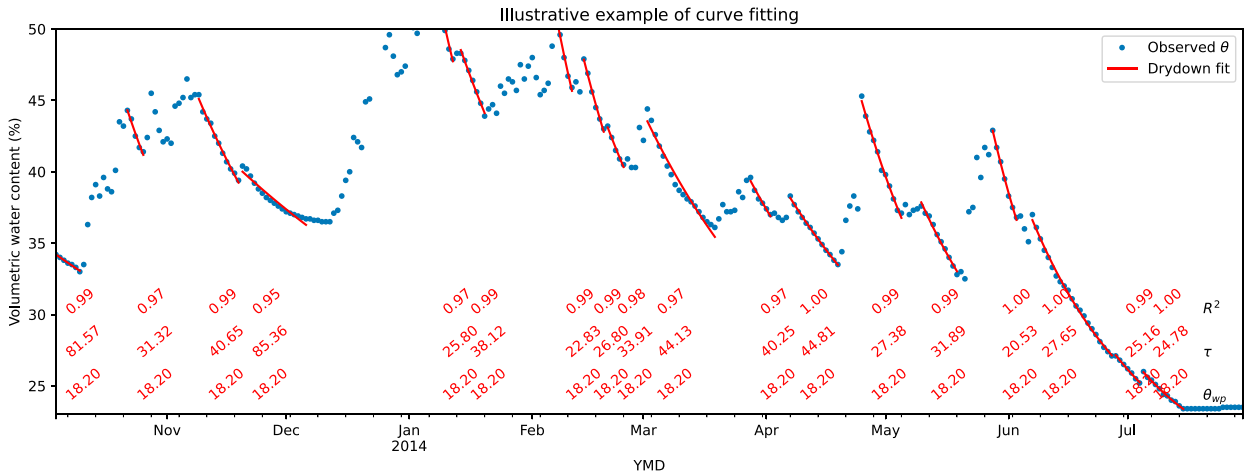
FIG. 2. Illustrative example of fitting τ for a COSMOS-UK site (Alice Holt, COSMOS measurements) based on Eq. (9). The R^2 values are reported as a measure of goodness-of-fit. Note that we fix the empirical wilting point to be the minimum value in the time series. Note that the numbers in red correspond to R^2, τ, and θ_{wp}; see labels at the right of the plot.

In this study, a drydown event is primarily defined as having 5 or more consecutive days of decreasing soil moisture. An advantage of this approach is that it does not depend on other time series (e.g., rainfall). Consistent with McColl et al. (2017), the drydown is then only kept if the coefficient of determination (R^2) of the exponential fit is at least 0.7. We have also removed drydown events with $\tau > 100$ days. This upper bound was implemented since drying events with τ exceeding this value would represent very slow drying or no drying at all which could be due to artificial water sourced from irrigation, too weak solar radiation in winter for soil evaporation, or no storage of soil moisture in regions of shallow groundwater table and slow drainage. These criteria are used when identifying drydowns in both the modeled and observed time series. No further filtering of drydowns is undertaken. We repeat this for the time series for each grid cell of each data products.

Alternatively, we can also define drydown events on the basis of rainless days (e.g., Raoult et al. 2021). A rainless day is defined as daily rainfall less than 1 mm and a drydown event has a minimum duration of 5 days. We note that in some studies, an initial increment is required to ensure enough water is in the soil and the drydown is driven by evapotranspiration (Shellito et al. 2016; Ruscica et al. 2020). This threshold is not used here because (i) some events with smaller initial increase will be discarded, and (ii) the second of two back-to-back drydown events will be discarded. Other authors (e.g., Raoult et al. 2021) have also opted not to include such criteria. They found that such criteria were more likely to exclude drydowns and that five dry days were sufficient to ensure an exponentially decaying drying of the soils.

3. Results

a. Comparison of soil moisture dynamics at COSMOS sites

All the data products considered have different assumptions, driving data (if applicable), and effective depths. This causes the soil moisture time series, albeit all tracking seasonality well, to vary greatly in values and the degree of fluctuations (see example at Alice Holt in Fig. 3). In particular, G2G and TCM have much bigger soil moisture ranges than the others and they both show a ~25% decrease in soil moisture from March to May 2017 at Alice Holt. This is further illustrated in Fig. 4, where the median Pearson's R between data product pairs (across sites) are all above 0.65 (ignoring CHESS$_{200}$, which is for deep soil moisture) but the Lin's concordance correlation coefficient (LCC) are very low. Higher LCC are seen between CHESS layers, CHESS and TCM, and between COSMOS and SMUK. In particular, CHESS$_{10}$, CHESS$_{25}$, and CHESS$_{adj}$ reproduce among themselves almost perfectly, indicating very limited interaction with deeper layers. Higher LCC reflects shared data sources, e.g., part of the calibration of SMUK used in this study is based on COSMOS observations. A high LCC of 0.77 between soil moisture probes at two depths, as well as a high LCC of 0.58 and 0.61 between COSMOS and the probes are observed, indicating an effect of observational scales (i.e., gridded data versus sensors at sites). The ubRMSE metric can show how the values between products, on average, differ at each point in time and space. CHESS$_{10}$ and SMUK show the lowest ubRMSE against other data products.

Figure 3 highlights the drydown events defined by rain gauge data (i.e., rainless days). G2G and CHESS shows clean decay in θ in most of the rainless events, while the statistical model SMUK and satellite-merged product TCM show that for a majority of rainless events. COSMOS, however, shows stronger fluctuations and nondecreasing θ for a number of the rainless events. To handle this issue, an exponential moving average filter is applied to the COSMOS-UK daily data to obtain smoother soil moisture time series. Figure 3 also highlights the following behavior of drydown events detected based on decreasing soil moisture: (i) their timings and durations differ greatly between products, and (ii) smoothing can greatly increase the number of events detected.
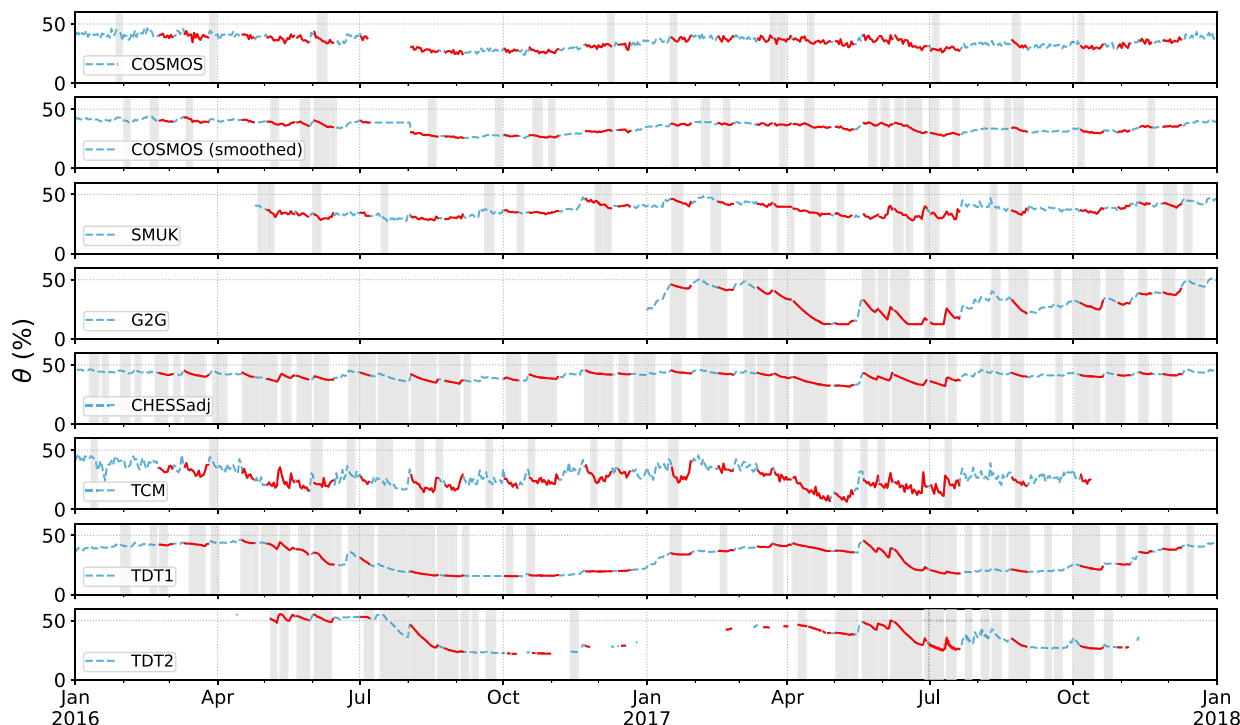
FIG. 3. Soil moisture time series from the various data products at Alice Holt (ALIC1). Drydown events based on COSMOS-UK rain gauge data at the site are highlighted in red dashed lines (the timings are identical for all products), while drydown events based on decreasing soil moisture are shaded in gray.

While it is expected there are disagreements between rain gauges and gridded rainfall products, their observations on the absence or presence of rain tend to be consistent. COS-MOS and TDT probes are the only products that are direct observation and do not take forcing data (which includes rainfall) into account. The above shows the advantage of identifying drydown events from individual soil moisture time series itself. Nevertheless, the definition based on rainfall can be useful when comparing τ from more than one product since all the products will have the same drydown events.

b. Comparison of drydown behavior of gridded products

Figure 5 shows the 1- or 2-km median τ of θ (i.e., $\overline{\tau}$) map over the United Kingdom for the different gridded products considered. The number of drydown events detected per cell corresponding to Fig. 5 is shown in the Fig. S1. Note only a few events are detected in the Scottish Highlands for TCM year-round and for SMUK and TCM in winter. In this section, CHESS$_{10}$ is the only CHESS product being considered. For the summer months (Fig. 5a), CHESS and SMUK show similar τ values ranging between 8 and 13 days for most of the United Kingdom. However, they seem to highlight different areas with higher $\overline{\tau}$ values (>15 days): SMUK shows higher $\overline{\tau}$ along the Welsh coast and along the Scottish Highlands, while for CHESS it is southeastern Scotland and southeastern England. CHESS also shows very low $\overline{\tau}$ values for northern Scotland, which is not observed in the other products. TCM is returning the lowest $\overline{\tau}$ values, where in most places it is

10 days or lower with even lower values along much of the English coast. This is potentially an effect of the low soil penetration depth of satellites (two out of three data sources in TCM are satellites) and hence fast drydowns in the top soil layer. Higher τ is observed in small parts of Scotland. The $\overline{\tau}$ map of G2G shows the highest level of spatial variation and much higher $\overline{\tau}$ values. Its $\overline{\tau}$ pattern has some resemblance of the HOST 1 km soil type dataset (https://www.ceh.ac.uk/data/hydrology-soil-types-1km-grid), which is one of G2G's input datasets, especially the depth to groundwater associated with the soil types (see Fig. S2). Note that G2G is not modeling surface soil moisture, but rather the soil moisture in the entire soil column (i.e., similar to all layers of CHESS combined). Note that in Fig. 3, G2G shows somewhat linear decay, which could explain the large τ values observed in this paper. It does not appear to have a soil moisture limitation on ET, as soil moisture decays linearly until the change suddenly becomes zero. While the G2G model includes an evaporation term, its soil moisture response could also be controlled by lateral drainage and percolation to groundwater.

Figure 5 also shows the median $\overline{\tau}$ map during winter (Fig. 5b) and for all seasons (Fig. 5c). On average, the range of winter $\overline{\tau}$ values are roughly twice of that in summer. Later in this paper, we show that this is because the main mechanism for drying in winter is drainage, while in the summer the soils are also dried by evaporation. The spatial pattern of median $\overline{\tau}$ maps also show differences across seasons. For much of England, median τ values exceeding 30 days are observed in winter, while for G2G,
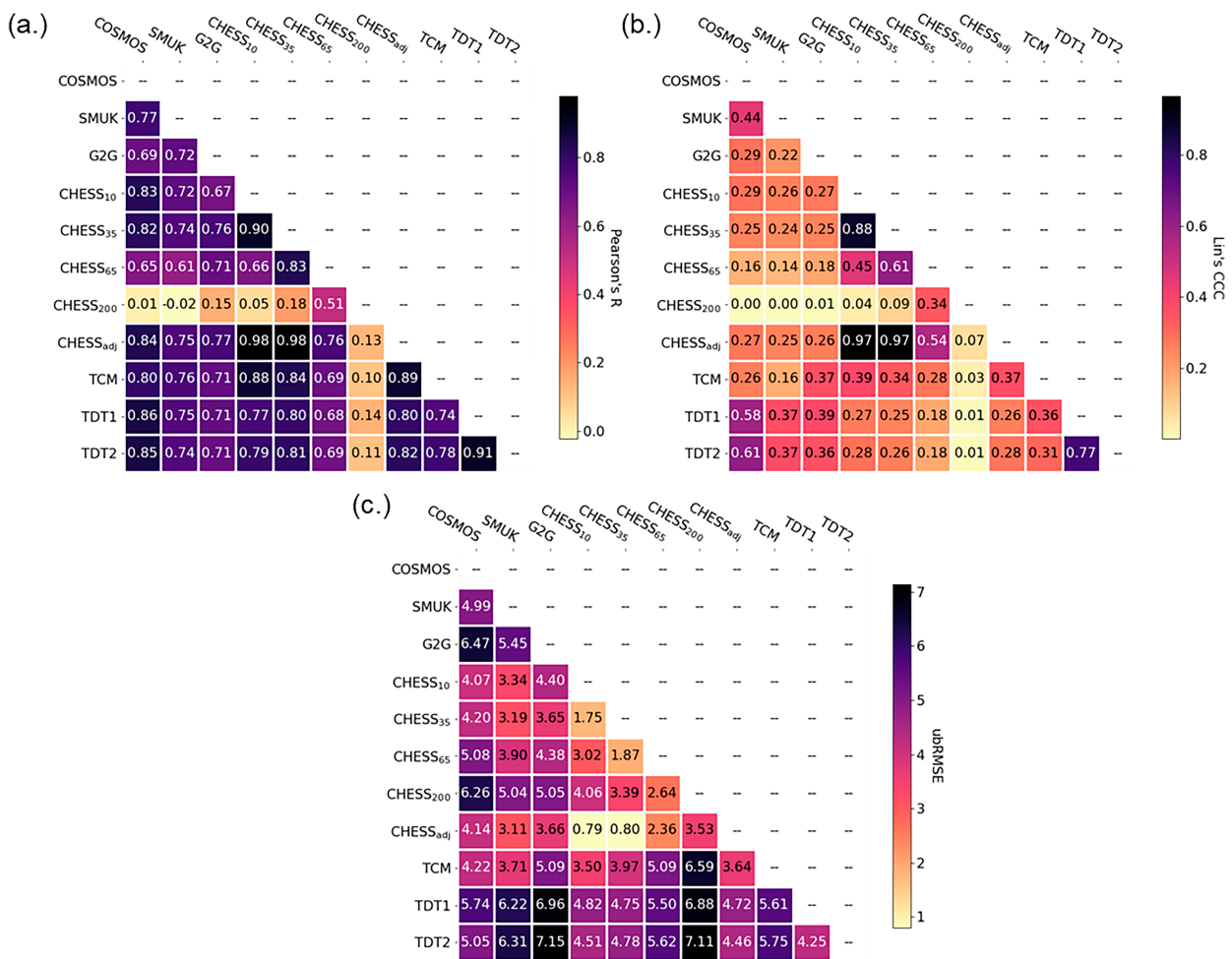
FIG. 4. Median (a) Pearson correlation and (b) Lin's concordance correlation coefficient (LCC) and (c) unbiased root-mean-square error across COSMOS sites. It is apparent that while many of the soil moisture are well correlated with each other, they reproduce each other poorly. Higher LCC reflects shared data sources, e.g., SMUK is conditioned on COSMOS measurements, as well as different layers of CHESS. TDT1 and TDT2 are soil moisture probes at 10- and 50-cm depth, respectively. CHESS$_{adj}$ is obtained by combining multiple CHESS layers according to the time-varying COSMOS sensing depths.

extremely high τ values are observed in many parts of the nation. Stronger spatial difference is observed in winter than summer by TCM, where $\bar{\tau}$ for much of England becomes higher, while τ remains very low (i.e., <5 days) for much of Scotland.

Figure 6 shows the probability density function (PDF) estimated based on kernel density estimation from each of the τ maps in Fig. 5. The spread of τ for each product is similar, except G2G has a very large spread. In the summer, SMUK and CHESS have similar PDFs with almost identical mean and median around 11 days, although SMUK has slightly higher spread. This indicates if there are attempts to merge the two products based on τ, bias correction may not be necessary. TCM gives the lowest estimates among the products with a mean τ of 7.86 days, which is not surprising as satellite products are sensing at a shallower depth compared to the other products. The τ values for 75% of the pixels are less than 13.4, 33.2, 12.6, and 9.0 days for SMUK, G2G, CHESS, and TCM, respectively. For winter months, $\bar{\tau}$ values generally

increase, with the standard deviation of $\bar{\tau}$ values for SMUK, CHESS, and TCM also increase by 2–3 times. The mean (and 75th percentile) $\bar{\tau}$ values of the pixels are 30.9 (37.1), 56.2 (73.3), 30.2 (37.3), and 16.5 (22.0) days for SMUK, G2G, CHESS, and TCM, respectively. Finally, the all-year distributions of median τ values resemble to the summer patterns more than the winter ones. Note that similar number of drydown events are found in SMUK and CHESS in summer and winter months. G2G shows up to 50% less drydown events than the others. This may be due to the fact that in many places, especially in the SE region, the soils represented in G2G are deeper and so are less sensitive to changes in rainfall. There are almost 30% more drydown events in summer than winter, while for TCM, there are 70% more drydown events in summer than winter (see Fig. S1). The PDFs of $\bar{\tau}$ for SMUK and CHESS almost perfectly overlap, while TCM and CHESS are also well correlated but the TCM estimate of $\bar{\tau}$ is typically half that of CHESS as it includes the satellite
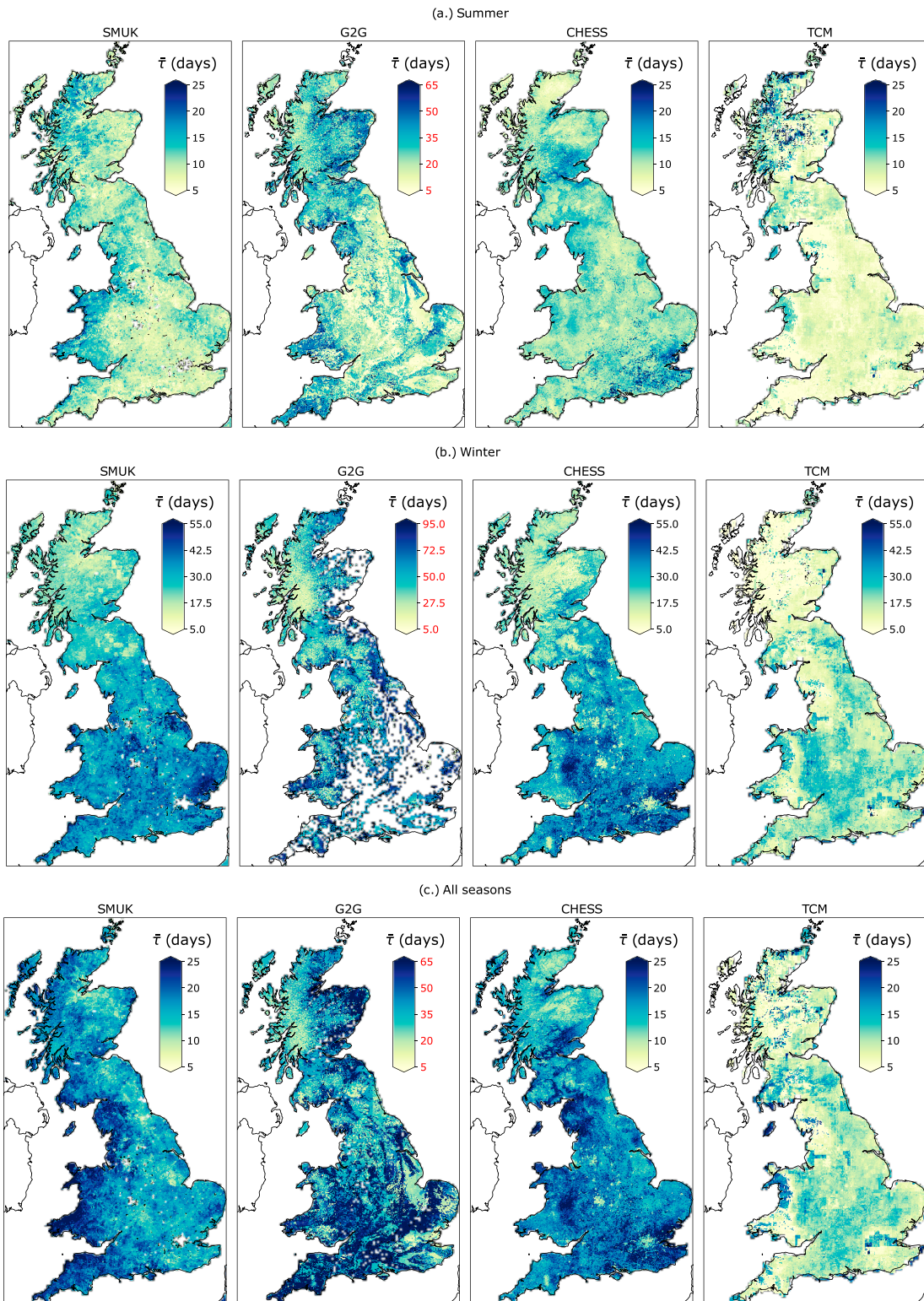
FIG. 5. Map of estimated median drydown time scale τ for the different 1- or 2-km gridded soil moisture products over Great Britain during (a) summer months (JJA), (b) winter months (DJF), and (c) the entire year: SMUK, G2G, CHESS (surface, i.e., top 10 cm), and TCM. The drydown events are determine by the decreasing soil moisture at each pixel. Note the color bar scales for G2G are different from the others. Note that in (b) areas in white indicate $\bar{\tau} > 100$ days and are thus excluded.
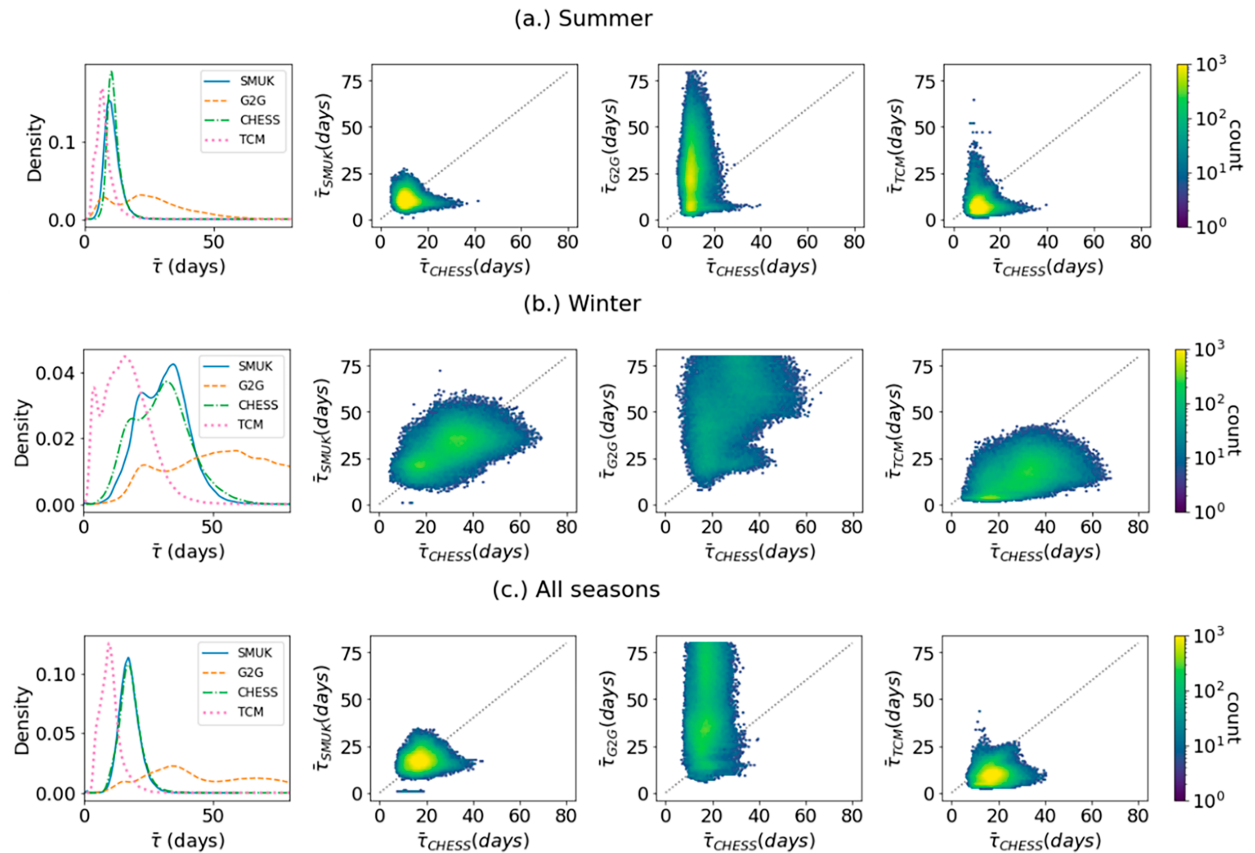
FIG. 6. Probability density function (PDF) for the estimated 1- or 2-km median drydown time scale $\bar{\tau}$ values for the different soil moisture products, and scatterplots of the estimated $\bar{\tau}$ for CHESS against other products for (a) summer, (b) winter, and (c) all seasons. The PDF for CHESS and SMUK in (c) are nearly coincident.

products that use a much shallower soil depth (1 cm). The mean (and 75th percentile) $\bar{\tau}$ values of the pixels are 17.9 (20.3), 47.7 (65.9), 17.8 (20.2), and 10.0 (11.8) days for SMUK, G2G, CHESS, and TCM, respectively.

With much ongoing peat restoration work to achieve net zero carbon emissions in the United Kingdom, it is of interest to understand the drydown properties of high carbon soils. We expect a higher value of $\bar{\tau}$ for high soil carbon areas as these peaty soils appears to retain water better compared to mineral soils. While those areas (e.g., Scottish Highlands) usually has higher absolute soil moisture values than the rest of the United Kingdom, their $\bar{\tau}$ values tend to be considerably lower than the rest of the United Kingdom (with the exception of SMUK). This is further demonstrated by the negative Spearman's rank correlations between a gridded soil carbon map and $\bar{\tau}$ maps in Table 3.

For both SMUK and CHESS, while $\bar{\tau}$ is uniformly low for most of the United Kingdom in summer ($\leq$10 days), $\bar{\tau}$ is higher in winter. This is expected as the drydown is likely to be much quicker in summer with the added drying effect of evaporation. In the winter, there also appears to be an influence of the urban areas in these two products which gives a faster drydown (lower $\bar{\tau}$) in the cities of London and Birmingham. For CHESS, urban areas are represented as having a

near-impermeable surface, so very little water enters the soils. This is in agreement with Jongen et al. (2022) in their observations of ET recessions in urban areas. Figure 7 summarizes the effect of land cover on $\bar{\tau}$. For G2G, as expected, $\bar{\tau}$ is high for all land cover types and a large range is observed. For arable land use, $\bar{\tau}$ tend to be lower than others for SMUK and CHESS, while higher for G2G and TCM. The comparison of $\bar{\tau}$ between woodlands and grasslands is important as it may indicate whether or not woodland restoration will alter the land's response to changing soil moisture. For CHESS, higher $\bar{\tau}$ is observed in broadleaf woodland than grasslands, followed by coniferous woodland. Martínez-de la Torre et al. (2019b) found that decay time scales are longer for trees than for grasslands. Meanwhile, for SMUK, higher $\bar{\tau}$ is observed in

TABLE 3. Spearman's rank correlation coefficient and Pearson's correlation between gridded values of $\bar{\tau}$ and topsoil carbon estimates.

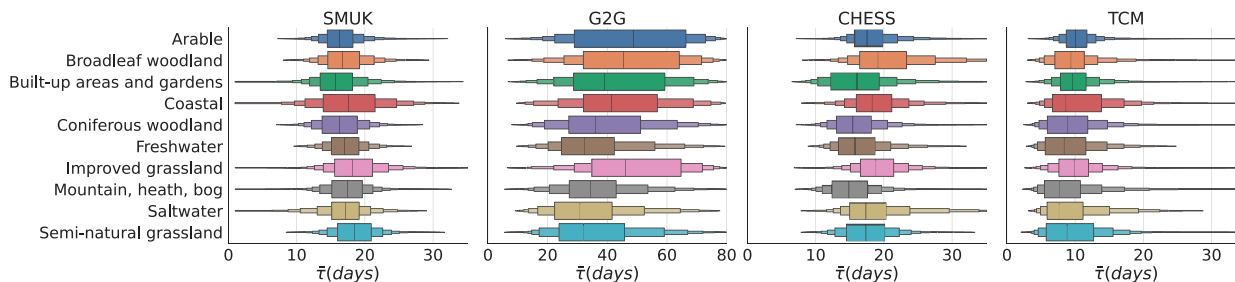| Product	Spearman's	Pearson's
SMUK	0.1566	0.0483
G2G	−0.2542	−0.2904
CHESS	−0.2127	−0.2510
TCM	−0.1913	0.0056

FIG. 7. Boxplot of $\bar{\tau}$ values in Fig. 5c grouped by Land Cover Map 2015 dominant class (Rowland et al. 2017).

improved and seminatural grassland than broadleaf and coniferous woodlands.

c. Comparison of drydown behavior at COSMOS-UK sites

When comparing drydown at COSMOS-UK site level, we focus on individual drydown events at individual sites. This can be achieved by plotting Gantt charts of the identified drydown events and color-code the bars with their τ values (Figs. 8a,b), where each horizontal bar represents a drydown event. In this section, CHESS data are adjusted to COSMOS depths (i.e., CHESS$_{adj}$). For brevity, we have only included the results for CHESS and COSMOS here, while the Gantt charts for the other data products are provided in Fig. S3. Note that the drydown events identified in CHESS$_{adj}$, G2G, TDT1, and TDT2, are considerably longer than those in SMUK, TCM (and its constitutive satellite products), and COSMOS. In all datasets, τ is strongly influenced by seasonality—low in summer while being very high (>40 days) in winter. The CHESS data also shows strong temporal coherence of τ values across sites, while the duration of summer drydown events tend to decrease with increasing latitudes. Figure 8a also shows interesting features such as the onset of a drydown events that affects all sites at the same time in June 2017, which indicates the termination of a rainfall event that affected the entire United Kingdom in CHESS's forcing data. Figure 9 shows the excess soil moisture at the COSMOS-UK sites and it shows the similar strong seasonality effects in Fig. 8a, suggesting a switch from a more energy-limited to a more water-limited regime from winter to summer. In winter drainage is more likely to be the only process for soil moisture decay, while in summer there are considerable contributions from both drainage and evaporation. The latitude of the site appears to have negligible effects on regime transition. Note the onset times are different for 2016 and 2017, but they are similar across sites in a particular year. Works on the changes in the timing of soil drying in a year under changing climate can help derive the implications of such change in regimes (Kay et al. 2022).

While the use of rainless days to define drydown events would require an additional data source, it is nonetheless useful as it defines the same events for different products, thus allowing a comparison of τ among them (e.g., Raoult et al. 2021). Figure S5 shows a Gantt chart of drydown events determined by the absence of rain and the two plots are colored by τ values estimated with adjusted CHESS and COSMOS-UK soil moisture during those events, respectively. Since the

events are identical, the bar locations in Fig. S5 are identical. Comparison with Fig. 8 shows the use of a rainfall-based approach identify fewer drydown events than the CHESS soil moisture–based approach. The lower τ values in the summer and autumn are also observed here. The τ values obtained from COSMOS-UK are generally greater than that from CHESS (in many cases more than 10 days), although this can be attributed to nondecreasing COSMOS-UK τ on rainless days. For both Fig. S5 and Fig. 8a, lower τ (i.e., <20 days) values are observed at sites well into October in 2016 but not in 2017, reflecting the difference in meteorological behavior between years. This is in agreement with excess soil moisture patterns (Fig. 9), indicating a strong effect of evaporative demands.

Figure 10 shows a scatterplot between τ values estimated by COSMOS-UK and CHESS (adjusted to COSMOS depths). The points are colored by the latitude of the COSMOS-UK site and the size of the points are proportional to the duration of the drydown event. The τ values estimated by the two products are well correlated, and similar to Raoult et al. (2021), we observe a bias for in situ observations (i.e., COSMOS-UK) to have a greater τ than LSM (i.e., CHESS). Note that this plot only shows a small proportion of the identified drydown events, since we have only included events where drydown fits have $R^2 \geq 0.7$ for both products. There is no noticeable latitude effect on τ and while sometimes τ pairs of the same site are close together, it is not necessarily the case. Longer drydown events tend to have a higher τ value. Figure S6 also shows that τ values tend to be higher when the start of the drydown events deviates from midyear, while Fig. S7 shows that the bias and spread in the 1:1 plot is mostly contributed by the most dominant land cover type and soil type at COSMOS-UK sites: improved grassland and mineral soil. Table 4 shows a similar analysis to Fig. 10 for all data product pairs. COSMOS versus TCM has the slope and Pearson's correlation closest to 1.0, while TDT probes tend to return smaller τ values than other products.

4. Discussions

With the rapid increase in the availability of soil moisture data products, many recent studies have compared soil moisture values from remote sensing, model, and ground observations data, e.g., with the soil water index (SWI) filter (Beck et al. 2021) or in the annual scale (Deng et al. 2020). In this work, we provide a first-of-its-kind comparison of drydown behavior of 1–2-km and point soil moisture across multiple
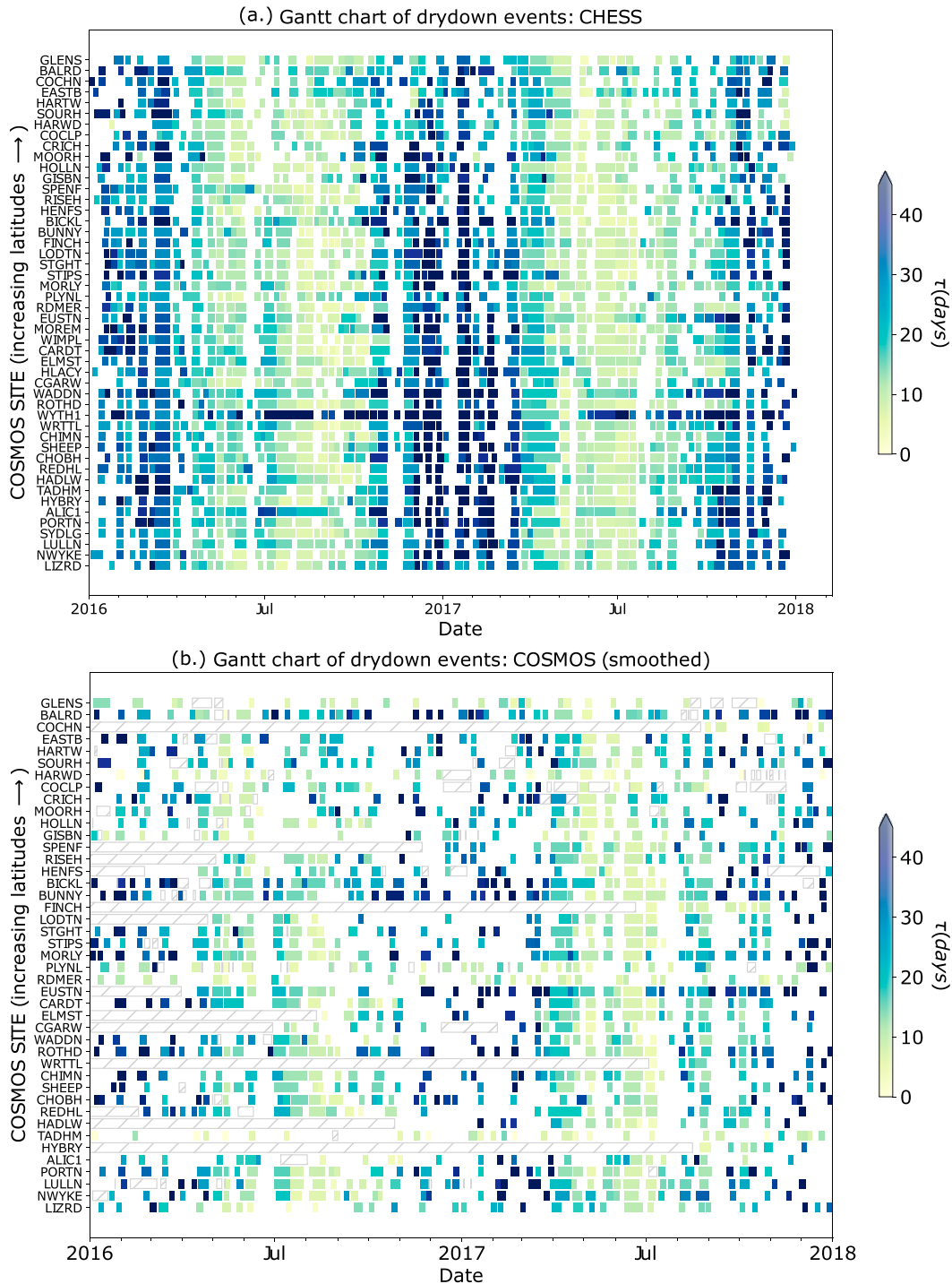
FIG. 8. Gantt chart of soil moisture drydown events at COSMOS-UK sites (ordered by increasing latitudes) based on (a) depth-adjusted CHESS_adj and (b) COSMOS-UK soil moisture observations. A gray hatched box denotes periods with missing data.

types of products at a national scale. The 1–2-km gridded products are at a scale relevant to weather and climate models as well as land management. Comparing and understanding the drydown behavior of the different products will enable us

to use the right soil moisture product for the right application, drive improvements in the representation of soil moisture drydown in models and help us create a flexible tool for evaluating soil moisture models.
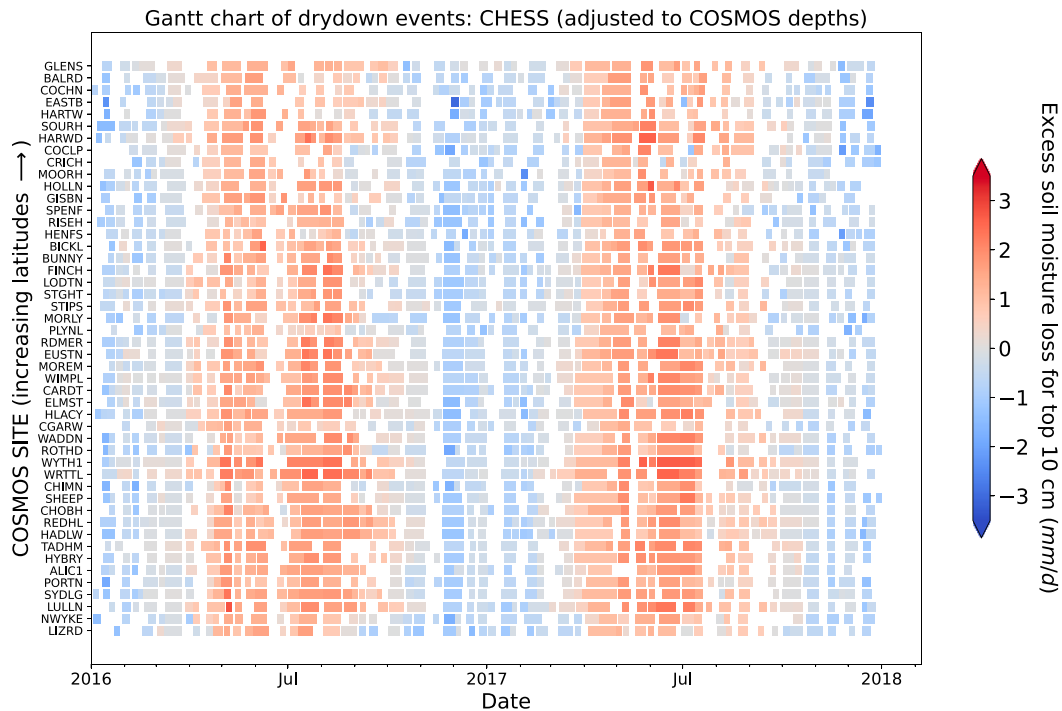
FIG. 9. As in Fig. 8a, but colored by daily average excess soil moisture loss, considering the top 10 cm of the soil column.

Analyzing almost 10 years of θ drydown globally, Raoult et al. (2022) showed that merging algorithms can lead to fewer drydown events detected, although drydown time scales are mostly unchanged. They also showed that detection based on external precipitation time series, rather than soil moisture

time series, lead to the detection of far fewer events and longer drydown time scales. Our analysis also shows that different methods create different number of drydown events detected. However, we have not observed fewer drydown events in the TCM product despite it being a merged product. While it has been shown vertically integrated (from the surface to 60 cm) soil moisture time series and its shallow (5 cm) counterpart has large mutual information and the former can be effectively duplicated by the low-pass transformation of the former (Qiu et al. 2014), we show that the representative depths of the different products (which can be spatially and temporally varying for some) lead to significantly different
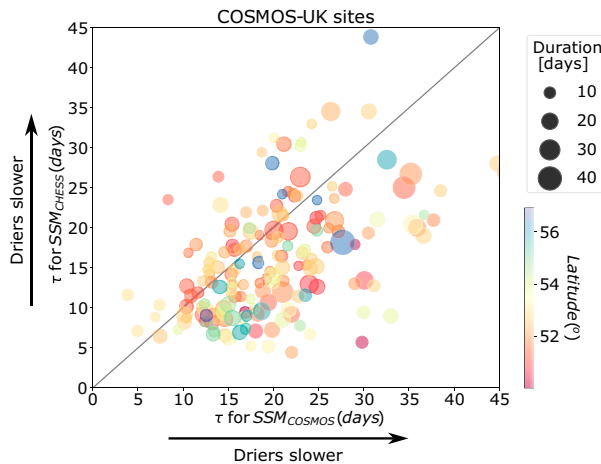

FIG. 10. Bubble plot showing the CHESS modeled (adjusted to COSMOS depths) vs observed COSMOS τ values at COSMOS-UK sites. The length (in days) of each drydown period (i.e., number of days with no rain) over which the exponential is fitted is represented by the size of the dot. Note that only pairs for $R^2 \geq 0.7$ for both data products are included. The color of the bubbles represents latitude.

TABLE 4. Slope and Pearson's correlation (R) of τ for pairs of data products. Drydown events are defined by lack of rainfall so they are identical for all products. Note that SMUK is not included because only a few pairs are available.

DF1	DF2	Number of pairs	Slope	R
COSMOS (smoothed)	CHESS_adj	330	0.7134	0.5606
COSMOS (smoothed)	TCM	119	0.8992	0.6860
COSMOS (smoothed)	TDT1	245	0.2917	0.4770
COSMOS (smoothed)	TDT2	259	0.2654	0.4288
CHESS_adj	TCM	165	0.6926	0.6484
CHESS_adj	TDT1	341	0.2069	0.3518
CHESS_adj	TDT2	344	0.2143	0.3637
TCM	TDT1	89	0.1122	0.2596
TCM	TDT2	99	0.0863	0.2418
TDT1	TDT2	304	0.6933	0.6693

drydown estimates. For instance, G2G soil moisture represents the depth-averaged soil moisture over a range of soil column depths across the United Kingdom, ranging from a few centimeters to several meters (Kay et al. 2022), while CHESS uses the same soil depth for the whole of the United Kingdom. Meanwhile, COSMOS observations and ASCAT sense greater depths when soils are dry (Zreda et al. 2008; Wagner et al. 2013) because water is a strong absorber of both low-frequency microwaves and cosmic-ray neutrons. Recently, COSMOS-UK data have been corrected to depths comparable to satellite sensing depths (1 cm) to aid their comparisons using Hydrus-1D modeling (Beale et al. 2021). This study shows that, since the drying time is so sensitive to soil moisture depth, a similar strategy to normalize soil moisture products to the same depth may be useful to yield a standardized "surface" soil moisture.

In their global satellite-based study, McColl et al. (2017) found that τ increases with soil sand content (consistent with soil suction) and decreases with aridity (i.e., higher water demand), while attributing unexplained variance to not-well-characterized vegetation. Our work similarly shows a decrease in τ in the summer due to higher water demand. Focusing on CONUS with better vegetation characterization, Shellito et al. (2018) reports that drying of surface soil moisture observed by SMAP satellite is faster than that simulated by the NOAH LSM, which has very similar soil layers as JULES. SMAP drying is fastest when surface soil moisture levels are high, potential evaporation is high, and when vegetation cover is low. Soil texture plays a minor role in SMAP drying rates. Our results confirm that the drying rates of satellite soil moisture (i.e., TCM, where two of the three data sources are satellites) is faster than LSM (i.e., CHESS) due to differences in sensing depths. We also show that the drydown is a strongly affected by potential evaporation. Any benchmarking or evaluation of models should therefore be carried out within times or places where the potential evaporation is similar.

Although the work has shown a way forward in bringing together different datasets, there remain some issues that need to be addressed before it is adopted as a standard data-model benchmark. For instance, some of the gridded datasets are not very long, and so are of reduced value. This may explain why we do not have a strong conclusion about the role of soil type and land cover type on the drying times. It is also true that the United Kingdom does not have long or consistent dry periods to explore and establish this method. We also do not have the soil properties at the soil moisture sensing sites which would enable us to confirm the relationship between drying times and soil type. It is recommended that the methods would be applied again in a region with stronger and longer drying periods to establish the importance of soil and vegetation on this landscape property.

It is worth noting there is a rich body of literature on the recessions in streamflow and ET. Streamflow recession analysis seeks to make inference to watershed properties directly from streamflow records (Troch et al. 2015), which is very similar to the goal of θ drydown analysis. The formulation by Kirchner (2009) allow a wider class of storage–discharge relationships, which may be transferrable to the modeling of θ versus $d\theta/dt$ relationships. Recently, Kim et al. (2023) shows machine learned individual flow

recession curves converge to a common attractor, which may present a novel way to analyze θ drydown as well. The study of τ in θ has been closely associated with the study of τ in ET. The two stages of drying in ET was proposed by Brutsaert and Chen (1995), which is later also used in soil moisture analysis. Lohmann and Wood (2003) found the ET time scale of 16 land surface schemes varied greatly. Teuling et al. (2006) reported observed time scales of ET response to θ and argued longer τ for ET represents weaker ET sensitivity (e.g., seasonal drought/woody vegetation). Koster and Suarez (2001) studied the memory of soil moisture in climate models and found that it is controlled by the relative strengths of four terms: 1) seasonality in the statistics of the atmospheric forcing, 2) the variation of evaporation with soil moisture, 3) the variation of runoff with soil moisture, and 4) correlation between the atmospheric forcing and antecedent soil moisture, as perhaps induced by land–atmosphere feedback. Boese et al. (2019) used ET drydown events to assess if and how decreasing soil water availability modifies water use efficiency at ecosystem scale. Carbon-flux coupling under water-limiting conditions could contribute to the land use effects on soil moisture drydown we observe in this work. In summary, we advocate for a more comprehensive approach to study τ in different components of the water cycle.

5. Conclusions

The critical role that soil moisture drydown plays in water availability and the land surface response and feedbacks with the atmosphere have long been established. However, it has remained difficult to find soil moisture observations at the right scale to evaluate models of this important property. Attempts to blend high-resolution satellite products at 1–2-km scale and point observations at sites struggle with issues around the high level of heterogeneity of the soil properties, and the strong difference in depth being "seen" by the different sensors (typically satellite sensors see only the top of the surface, point sensors see down to tens of centimeters and models can be looking at the top 1 m of soil). In this analysis we used a simple metric to describe soil drydown that can be calculated for all soil moisture products, including sensors at COSMOS-UK sites, models and new satellite–model blended products. We show that soil moisture drydown is highly dependent on the soil depth over which the product is averaged. This indicates that normalizing the soil moisture to a fixed depth would massively improve our ability to test models against data. The drydown also exhibits strong seasonal dependencies controlled by PE, which we show to be governed by excess soil moisture (i.e., ESM = $\theta\Delta z$ − PEΔt). Therefore benchmarking should also be done within seasons, not for the whole year.

Our findings allow an improved understanding on the characteristics and patterns of τ obtained from different U.K. soil moisture products at different scales, provide a basis to improve the representation of soil moisture drydown in modeled products, and enable us to derive a new way to benchmark modeled soil moisture.

Data availability statement. The following datasets used in this study are hosted by the NERC EDS Environmental Information Data Centre (EIDC, hosted by UKCEH) under the Open Government License: COSMOS-UK (Stanley et al. 2021), its data are also available to view in the U.K. Water Resources Portal (https://eip.ceh.ac.uk/hydrology/water-resources/); CHESS- PE (Robinson et al. 2020b); CHESS-Met (Robinson et al. 2020a); CHESS-land soil moisture (Martinez-de la Torre et al. 2018); TCM (Tanguy et al. 2022); G2G (Kay et al. 2021b); Land cover map 2015 (Rowland et al. 2017). The following datasets are currently available via the JASMIN public data store: SMUK: https://gws-access.jasmin.ac.uk/public/dare_uk/smuk/2022/.

REFERENCES

Abbaszadeh, P., H. Moradkhani, and X. Zhan, 2019: Downscaling SMAP radiometer soil moisture over the CONUS using an ensemble learning method. *Water Resour. Res.*, **55**, 324–344, https://doi.org/10.1029/2018WR023354.

Akbar, R., D. J. Short Gianotti, K. A. McColl, E. Haghighi, G. D. Salvucci, and D. Entekhabi, 2018a: Estimation of landscape soil water losses from satellite observations of soil moisture. *J. Hydrometeor.*, **19**, 871–889, https://doi.org/10.1175/JHM-D-17-0200.1.

——, D. Short Gianotti, K. A. McColl, E. Haghighi, G. D. Salvucci, and D. Entekhabi, 2018b: Hydrological storage length scales represented by remote sensing estimates of soil moisture and precipitation. *Water Resour. Res.*, **54**, 1476–1492, https://doi.org/10.1002/2017WR021508.

Babaeian, E., M. Sadeghi, S. B. Jones, C. Montzka, H. Vereecken, and M. Tuller, 2019: Ground, proximal and satellite remote sensing of soil moisture. *Rev. Geophys.*, **57**, 530–616, https://doi.org/10.1029/2018RG000618.

Bauer-Marschallinger, B., and Coauthors, 2018: Soil moisture from fusion of scatterometer and SAR: Closing the scale gap with temporal filtering. *Remote Sens.*, **10**, 1030, https://doi.org/10.3390/rs10071030.

Beale, J., T. Waine, J. Evans, and R. Corstanje, 2021: A method to assess the performance of SAR-derived surface soil moisture products. *IEEE J. Sel. Top. Appl. Earth Obs. Remote Sens.*, **14**, 4504–4516, https://doi.org/10.1109/JSTARS.2021.3071380.

Beck, H. E., and Coauthors, 2021: Evaluation of 18 satellite- and model-based soil moisture products using in situ measurements from 826 sensors. *Hydrol. Earth Syst. Sci.*, **25**, 17–40, https://doi.org/10.5194/hess-25-17-2021.

Beff, L., T. Günther, B. Vandoorne, V. Couvreur, and M. Javaux, 2013: Three-dimensional monitoring of soil water content in a maize field using electrical resistivity tomography. *Hydrol. Earth Syst. Sci.*, **17**, 595–609, https://doi.org/10.5194/hess-17-595-2013.

Bell, V. A., A. L. Kay, R. G. Jones, R. J. Moore, and N. S. Reynard, 2009: Use of soil data in a grid-based hydrological model to estimate spatial variation in changing flood risk across the UK. *J. Hydrol.*, **377**, 335–350, https://doi.org/10.1016/j.jhydrol.2009.08.031.

——, ——, H. N. Davies, and R. G. Jones, 2016: An assessment of the possible impacts of climate change on snow and peak river flows across Britain. *Climatic Change*, **136**, 539–553, https://doi.org/10.1007/s10584-016-1637-x.

Berg, A., B. R. Lintner, K. L. Findell, S. Malyshev, P. C. Loikith, and P. Gentine, 2014: Impact of soil moisture–atmosphere interactions on surface temperature distribution. *J. Climate*, **27**, 7976–7993, https://doi.org/10.1175/JCLI-D-13-00591.1.

——, and Coauthors, 2016: Land–atmosphere feedbacks amplify aridity increase over land under global warming. *Nat. Climate Change*, **6**, 869–874, https://doi.org/10.1038/nclimate3029.

Best, M. J., and Coauthors, 2011: The Joint UK Land Environment Simulator (JULES), model description – Part 1: Energy and water fluxes. *Geosci. Model Dev.*, **4**, 677–699, https://doi.org/10.5194/gmd-4-677-2011.

Blonquist, J. M., Jr., S. B. Jones, and D. A. Robinson, 2005: A time domain transmission sensor with TDR performance characteristics. *J. Hydrol.*, **314**, 235–245, https://doi.org/10.1016/j.jhydrol.2005.04.005.

Blyth, E. M., A. Martínez-de la Torre, and E. L. Robinson, 2019: Trends in evapotranspiration and its drivers in Great Britain: 1961 to 2015. *Prog. Phys. Geogr.*, **43**, 666–693, https://doi.org/10.1177/0309133319841891.

——, and Coauthors, 2021: Advances in land surface modelling. *Curr. Climate Change Rep.*, **7**, 45–71, https://doi.org/10.1007/s40641-021-00171-5.

Boese, S., M. Jung, N. Carvalhais, A. J. Teuling, and M. Reichstein, 2019: Carbon–water flux coupling under progressive drought. *Biogeosciences*, **16**, 2557–2572, https://doi.org/10.5194/bg-16-2557-2019.

Bogena, H. R., and Coauthors, 2022: COSMOS-Europe: A European network of cosmic-ray neutron soil moisture sensors. *Earth Syst. Sci. Data*, **14**, 1125–1151, https://doi.org/10.5194/essd-14-1125-2022.

Bomblies, A., and E. A. B. Eltahir, 2009: Assessment of the impact of climate shifts on malaria transmission in the Sahel. *EcoHealth*, **6**, 426–437, https://doi.org/10.1007/s10393-010-0274-5.

Bonan, G. B., and L. M. Stillwell-Soller, 1998: Soil water and the persistence of floods and droughts in the Mississippi River basin. *Water Resour. Res.*, **34**, 2693–2701, https://doi.org/10.1029/98WR02073.

Boorman, D. B., J. M. Hollis, and A. Lilly, 1995: Hydrology of soil types: A hydrologically-based classification of the soils of United Kingdom. IH Tech. Rep. 126, 146 pp., https://nora.nerc.ac.uk/id/eprint/7369/.

Brunetti, G., J. Šimůnek, H. Bogena, R. Baatz, J. A. Huisman, H. Dahlke, and H. Vereecken, 2019: On the information content of cosmic-ray neutron data in the inverse estimation of soil hydraulic properties. *Vadose Zone J.*, **18**, 1–24, https://doi.org/10.2136/vzj2018.06.0123.

Brutsaert, W., and D. Chen, 1995: Desorption and the two stages of drying of natural tallgrass prairie. *Water Resour. Res.*, **31**, 1305–1313, https://doi.org/10.1029/95WR00323.

Chen, F., W. T. Crow, R. Bindlish, A. Colliander, M. S. Burgin, J. Asanuma, and K. Aida, 2018: Global-scale evaluation of SMAP, SMOS and ASCAT soil moisture products using triple collocation. *Remote Sens. Environ.*, **214**, 1–13, https://doi.org/10.1016/j.rse.2018.05.008.

Cooper, E., E. Blyth, H. Cooper, R. Ellis, E. Pinnington, and S. J. Dadson, 2021: Using data assimilation to optimize pedotransfer functions using field-scale in situ soil moisture observations. *Hydrol. Earth Syst. Sci.*, **25**, 2445–2458, https://doi.org/10.5194/hess-25-2445-2021.

Cooper, H. M., and Coauthors, 2021: COSMOS-UK: National soil moisture and hydrometeorology data for environmental science research. *Earth Syst. Sci. Data*, **13**, 1737–1757, https://doi.org/10.5194/essd-13-1737-2021.

Dafflon, B., J. Irving, and K. Holliger, 2009: Use of high-resolution geophysical data to characterize heterogeneous aquifers: Influence of data integration method on hydrological predictions. *Water Resour. Res.*, **45**, W09407, https://doi.org/10.1029/2008WR007646.

Deng, Y., and Coauthors, 2020: Comparison of soil moisture products from microwave remote sensing, land model, and reanalysis using global ground observations. *Hydrol. Processes*, **34**, 836–851, https://doi.org/10.1002/hyp.13636.

de Wit, A. J. W., and C. A. van Diepen, 2008: Crop growth modelling and crop yield forecasting using satellite-derived meteorological inputs. *Int. J. Appl. Earth Obs. Geoinf.*, **10**, 414–425, https://doi.org/10.1016/j.jag.2007.10.004.

Dirmeyer, P. A., Z. Wang, M. J. Mbuh, and H. E. Norton, 2014: Intensified land surface control on boundary layer growth in a changing climate. *Geophys. Res. Lett.*, **41**, 1290–1294, https://doi.org/10.1002/2013GL058826.

D'Odorico, P., F. Laio, A. Porporato, and I. Rodriguez-Iturbe, 2003: Hydrologic controls on soil carbon and nitrogen cycles. II. A case study. *Adv. Water Resour.*, **26**, 59–70, https://doi.org/10.1016/S0309-1708(02)00095-7.

Dong, J., R. Akbar, D. J. Short Gianotti, A. F. Feldman, W. T. Crow, and D. Entekhabi, 2022: Can surface soil moisture information identify evapotranspiration regime transitions? *Geophys. Res. Lett.*, **49**, e2021GL097697, https://doi.org/10.1029/2021GL097697.

Dorigo, W., and Coauthors, 2017: ESA CCI soil moisture for improved Earth system understanding: State-of-the art and future directions. *Remote Sens. Environ.*, **203**, 185–215, https://doi.org/10.1016/j.rse.2017.07.001.

Entekhabi, D., and Coauthors, 2010: The Soil Moisture Active Passive (SMAP) mission. *Proc. IEEE*, **98**, 704–716, https://doi.org/10.1109/JPROC.2010.2043918.

Evans, J. G., and Coauthors, 2016: Soil water content in southern England derived from a cosmic-ray soil moisture observing system – COSMOS-UK. *Hydrol. Processes*, **30**, 4987–4999, https://doi.org/10.1002/hyp.10929.

Fatichi, S., C. Pappas, and V. Y. Ivanov, 2016: Modeling plant–water interactions: An ecohydrological overview from the cell to the global scale. *Wiley Interdiscip. Rev.: Water*, **3**, 327–368, https://doi.org/10.1002/wat2.1125.

Feldman, A. F., and Coauthors, 2023: Remotely sensed soil moisture can capture dynamics relevant to plant water uptake. *Water Resour. Res.*, **59**, e2022WR033814, https://doi.org/10.1029/2022WR033814.

Franz, T. E., M. Zreda, R. Rosolem, and T. P. A. Ferre, 2013: A universal calibration function for determination of soil moisture with cosmic-ray neutrons. *Hydrol. Earth Syst. Sci.*, **17**, 453–460, https://doi.org/10.5194/hess-17-453-2013.

Fuller, R. M., and Coauthors, 2002: Land Cover Map 2000 (1 km dominant aggregate class, GB). NERC Environmental Information Data Centre, accessed 31 January 2023, https://doi.org/10.5285/b8b8a266-9162-40d8-98a6-f44178d31543.

Ghosh, S., D. M. Bell, J. S. Clark, A. E. Gelfand, and P. G. Flikkema, 2014: Process modeling for soil moisture using sensor network data. *Stat. Methodol.*, **17**, 99–112, https://doi.org/10.1016/j.stamet.2013.08.002.

Green, J. K., S. I. Seneviratne, A. M. Berg, K. L. Findell, S. Hagemann, D. M. Lawrence, and P. Gentine, 2019: Large influence of soil moisture on long-term terrestrial carbon uptake. *Nature*, **565**, 476–479, https://doi.org/10.1038/s41586-018-0848-x.

Gruber, A., W. A. Dorigo, W. Crow, and W. Wagner, 2017: Triple collocation-based merging of satellite soil moisture retrievals. *IEEE Trans. Geosci. Remote Sens.*, **55**, 6780–6792, https://doi.org/10.1109/TGRS.2017.2734070.

——, and Coauthors, 2020: Validation practices for satellite soil moisture retrievals: What are (the) errors? *Remote Sens. Environ.*, **244**, 111806, https://doi.org/10.1016/j.rse.2020.111806.

Haghighi, E., D. J. Short Gianotti, R. Akbar, G. D. Salvucci, and D. Entekhabi, 2018: Soil and atmospheric controls on the land surface energy balance: A generalized framework for distinguishing moisture-limited and energy-limited evaporation regimes. *Water Resour. Res.*, **54**, 1831–1851, https://doi.org/10.1002/2017WR021729.

Hallett, S. H., P. Thanigasalam, and J. M. Hollis, 1995: SEISMIC: A desktop information system for assessing the fate and behaviour of pesticides in the environment. *Comput. Electron. Agric.*, **13**, 227–242, https://doi.org/10.1016/0168-1699(95)00017-X.

Henrys, P. A., A. M. Keith, D. A. Robinson, and B. A. Emmett, 2012: Model estimates of topsoil carbon [Countryside Survey]. NERC Environmental Information Data Centre, accessed 31 January 2023, https://doi.org/10.5285/9e4451f8-23d3-40dc-9302-73e30ad3dd76.

Hough, M. N., and R. J. A. Jones, 1997: The United Kingdom Meteorological Office rainfall and evaporation calculation system: MORECS version 2.0-an overview. *Hydrol. Earth Syst. Sci.*, **1**, 227–239, https://doi.org/10.5194/hess-1-227-1997.

Humphrey, V., A. Berg, P. Ciais, P. Gentine, M. Jung, M. Reichstein, S. I. Seneviratne, and C. Frankenberg, 2021: Soil moisture–atmosphere feedback dominates land carbon uptake variability. *Nature*, **592**, 65–69, https://doi.org/10.1038/s41586-021-03325-5.

Jongen, H. J., and Coauthors, 2022: Urban water storage capacity inferred from observed evapotranspiration recession. *Geophys. Res. Lett.*, **49**, e2021GL096069, https://doi.org/10.1029/2021GL096069.

Kay, A. L., A. Griffin, A. C. Rudd, R. M. Chapman, V. A. Bell, and N. W. Arnell, 2021a: Climate change effects on indicators of high and low river flow across Great Britain. *Adv. Water Resour.*, **151**, 103909, https://doi.org/10.1016/j.advwatres.2021.103909.

——, A. C. Rudd, H. N. Davies, R. A. Lane, and V. A. Bell, 2021b: Grid-to-Grid model estimates of soil moisture for Great Britain and Northern Ireland driven by observed data (1980 to 2011). NERC EDS Environmental Information Data Centre, accessed 31 January 2023, https://doi.org/10.5285/c9a85f7c-45e2-4201-af82-4c833b3f2c5f.

——, R. A. Lane, and V. A. Bell, 2022: Grid-based simulation of soil moisture in the UK: Future changes in extremes and wetting and drying dates. *Environ. Res. Lett.*, **17**, 074029, https://doi.org/10.1088/1748-9326/ac7a4e.

Keller, V. D. J., and Coauthors, 2015: CEH-GEAR: 1 km resolution daily and monthly areal rainfall estimates for the UK for hydrological and other applications. *Earth Syst. Sci. Data*, **7**, 143–155, https://doi.org/10.5194/essd-7-143-2015.

Kerr, D. D., and T. E. Ochsner, 2020: Soil organic carbon more strongly related to soil moisture than soil temperature in

temperate grasslands. *Soil Sci. Soc. Amer. J.*, **84**, 587–596, https://doi.org/10.1002/saj2.20018.

Kim, M., H. H. Bauser, K. Beven, and P. A. Troch, 2023: Time-variability of flow recession dynamics: Application of machine learning and learning from the machine. *Water Resour. Res.*, **59**, e2022WR032690, https://doi.org/10.1029/2022WR032690.

Kirchner, J. W., 2009: Catchments as simple dynamical systems: Catchment characterization, rainfall-runoff modeling, and doing hydrology backward. *Water Resour. Res.*, **45**, W02429, https://doi.org/10.1029/2008WR006912.

Köhli, M., M. Schrön, M. Zreda, U. Schmidt, P. Dietrich, and S. Zacharias, 2015: Footprint characteristics revised for field-scale soil moisture monitoring with cosmic-ray neutrons. *Water Resour. Res.*, **51**, 5772–5790, https://doi.org/10.1002/2015WR017169.

Koster, R. D., and M. J. Suarez, 2001: Soil moisture memory in climate models. *J. Hydrometeor.*, **2**, 558–570, https://doi.org/10.1175/1525-7541(2001)002<0558:SMMICM>2.0.CO;2.

Krueger, E. S., T. E. Ochsner, D. M. Engle, J. D. Carlson, D. Twidwell, and S. D. Fuhlendorf, 2015: Soil moisture affects growing-season wildfire size in the southern Great Plains. *Soil Sci. Soc. Amer. J.*, **79**, 1567–1576, https://doi.org/10.2136/sssaj2015.01.0041.

Kurc, S. A., and E. E. Small, 2004: Dynamics of evapotranspiration in semiarid grassland and shrubland ecosystems during the summer monsoon season, central New Mexico. *Water Resour. Res.*, **40**, W09305, https://doi.org/10.1029/2004WR003068.

Lane, R. A., and A. L. Kay, 2021: Climate change impact on the magnitude and timing of hydrological extremes across Great Britain. *Front. Water*, **3**, 684982, https://doi.org/10.3389/frwa.2021.684982.

Levy, P. E., and COSMOS-UK Team, 2023: Mapping soil moisture across the UK: Assimilating cosmic-ray neutron sensors, remotely-sensed indices, rainfall radar and catchment water balance data in a Bayesian hierarchical model. *EGUsphere*, https://doi.org/10.5194/egusphere-2023-2041.

Lin, L. I.-K., 1989: A concordance correlation coefficient to evaluate reproducibility. *Biometrics*, **45**, 255–268, https://doi.org/10.2307/2532051.

Liu, J., F. Rahmani, K. Lawson, and C. Shen, 2022: A multiscale deep learning model for soil moisture integrating satellite and in situ data. *Geophys. Res. Lett.*, **49**, e2021GL096847, https://doi.org/10.1029/2021GL096847.

Lohmann, D., and E. F. Wood, 2003: Timescales of land surface evapotranspiration response in the PILPS phase 2(c). *Global Planet. Change*, **38**, 81–91, https://doi.org/10.1016/S0921-8181(03)00007-9.

Long, D., and Coauthors, 2019: Generation of spatially complete and daily continuous surface soil moisture of high spatial resolution. *Remote Sens. Environ.*, **233**, 111364, https://doi.org/10.1016/j.rse.2019.111364.

Lorenz, R., E. B. Jaeger, and S. I. Seneviratne, 2010: Persistence of heat waves and its link to soil moisture memory. *Geophys. Res. Lett.*, **37**, L09703, https://doi.org/10.1029/2010GL042764.

Martínez-de la Torre, A., E. M. Blyth, and E. L. Robinson, 2018: Water, carbon and energy fluxes simulation for Great Britain using the JULES land surface model and the climate hydrology and ecology research support system meteorology dataset (1961–2015) [CHESS-land]. NERC Environmental Information Data Centre, accessed 31 January 2023, https://doi.org/10.5285/c76096d6-45d4-4a69-a310-4c67f8dcf096.

——, ——, and G. P. Weedon, 2019a: Using observed river flow data to improve the hydrological functioning of the JULES land surface model (vn4.3) used for regional coupled modelling in Great Britain (UKC2). *Geosci. Model Dev.*, **12**, 765–784, https://doi.org/10.5194/gmd-12-765-2019.

——, ——, and E. L. Robinson, 2019b: Evaluation of drydown processes in global land surface and hydrological models using flux tower evapotranspiration. *Water*, **11**, 356, https://doi.org/10.3390/w11020356.

Maxwell, R. M., F. K. Chow, and S. J. Kollet, 2007: The groundwater–land-surface–atmosphere connection: Soil moisture effects on the atmospheric boundary layer in fully-coupled simulations. *Adv. Water Resour.*, **30**, 2447–2466, https://doi.org/10.1016/j.advwatres.2007.05.018.

McColl, K. A., W. Wang, B. Peng, R. Akbar, D. J. Short Gianotti, H. Lu, M. Pan, and D. Entekhabi, 2017: Global characterization of surface soil moisture drydowns. *Geophys. Res. Lett.*, **44**, 3682–3690, https://doi.org/10.1002/2017GL072819.

Meng, L., and S. M. Quiring, 2008: A comparison of soil moisture models using soil climate analysis network observations. *J. Hydrometeor.*, **9**, 641–659, https://doi.org/10.1175/2008JHM916.1.

Met Office, 2003: 1 km Resolution UK composite rainfall data from the Met Office NIMROD system. NCAS British Atmospheric Data Centre, accessed 31 January 2023, https://catalogue.ceda.ac.uk/uuid/27dd6ffba67f667a18c62de5c3456350.

——, 2016: NWP-UKV: Met Office UK atmospheric high resolution model data. Centre for Environmental Data Analysis, accessed 31 January 2023, https://catalogue.ceda.ac.uk/uuid/f47bc62786394626b665e23b658d385f.

——, D. Hollis, M. McCarthy, M. Kendon, and T. Legg, 2022: HadUK-Grid gridded climate observations on a 1km grid over the UK, v1.1.0.0 (1836–2021). NERC EDS Centre for Environmental Data Analysis, accessed 31 January 2023, https://doi.org/10.5285/bbca3267dc7d4219af484976734c9527.

O, S., and R. Orth, 2021: Global soil moisture data derived through machine learning trained with in-situ measurements. *Sci. Data*, **8**, 170, https://doi.org/10.1038/s41597-021-00964-1.

Oki, T., D. Entekhabi, and T. I. Harrold, 2004: The global water cycle. *The State of the Planet: Frontiers and Challenges in Geophysics*, R. S. J. Sparks and C. J. Hawkesworth, Eds., Wiley, 225–237.

Peng, J., and Coauthors, 2021a: A roadmap for high-resolution satellite soil moisture applications – Confronting product characteristics with user requirements. *Remote Sens. Environ.*, **252**, 112162, https://doi.org/10.1016/j.rse.2020.112162.

——, and Coauthors, 2021b: Estimation and evaluation of high-resolution soil moisture from merged model and Earth observation data in the Great Britain. *Remote Sens. Environ.*, **264**, 112610, https://doi.org/10.1016/j.rse.2021.112610.

Pinnington, E., and Coauthors, 2021: Improving soil moisture prediction of a high-resolution land surface model by parameterising pedotransfer functions through assimilation of SMAP satellite data. *Hydrol. Earth Syst. Sci.*, **25**, 1617–1641, https://doi.org/10.5194/hess-25-1617-2021.

Qiu, J., W. T. Crow, G. S. Nearing, X. Mo, and S. Liu, 2014: The impact of vertical measurement depth on the information content of soil moisture times series data. *Geophys. Res. Lett.*, **41**, 4997–5004, https://doi.org/10.1002/2014GL060017.

Rameshwaran, P., V. A. Bell, M. J. Brown, H. N. Davies, A. L. Kay, A. C. Rudd, and C. Sefton, 2022: Use of abstraction and discharge data to improve the performance of a national-scale hydrological model. *Water Resour. Res.*, **58**, e2021WR029787, https://doi.org/10.1029/2021WR029787.

Raoult, N., C. Ottlé, P. Peylin, V. Bastrikov, and P. Maugis, 2021: Evaluating and optimizing surface soil moisture drydowns in

the ORCHIDEE land surface model at In Situ locations. *J. Hydrometeor.*, **22**, 1025–1043, https://doi.org/10.1175/JHM-D-20-0115.1.

——, R. C. Ruscica, M. M. Salvia, and A. A. Sörensson, 2022: Soil moisture drydown detection is hindered by model-based rescaling. *IEEE Geosci. Remote Sens. Lett.*, **19**, 1–5, https://doi.org/10.1109/LGRS.2022.3178685.

Richards, L. A., 1931: Capillary conduction of liquids through porous mediums. *J. Appl. Phys.*, **1**, 318–333, https://doi.org/10.1063/1.1745010.

Robinson, D. A., S. B. Jones, J. M. Wraith, D. Or, and S. P. Friedman, 2003: A review of advances in dielectric and electrical conductivity measurement in soils using time domain reflectometry. *Vadose Zone J.*, **2**, 444–475, https://doi.org/10.2136/vzj2003.4440.

Robinson, E. L., E. M. Blyth, D. B. Clark, J. Finch, and A. C. Rudd, 2017: Trends in atmospheric evaporative demand in Great Britain using high-resolution meteorological data. *Hydrol. Earth Syst. Sci.*, **21**, 1189–1224, https://doi.org/10.5194/hess-21-1189-2017.

——, ——, ——, E. Comyn-Platt, and A. C. Rudd, 2020a: Climate hydrology and ecology research support system meteorology dataset for Great Britain (1961–2017) [CHESS-met]. NERC Environmental Information Data Centre, accessed 31 January 2023, https://doi.org/10.5285/2ab15bf0-ad08-415c-ba64-831168be7293.

——, ——, ——, ——, and ——, 2020b: Climate hydrology and ecology research support system potential evapotranspiration dataset for Great Britain (1961–2017) [CHESS-PE]. NERC Environmental Information Data Centre, accessed 31 January 2023, https://doi.org/10.5285/9116e565-2c0a-455b-9c68-558fdd9179ad.

Rodell, M., and Coauthors, 2004: The Global Land Data Assimilation System. *Bull. Amer. Meteor. Soc.*, **85**, 381–394, https://doi.org/10.1175/BAMS-85-3-381.

Rondinelli, W. J., B. K. Hornbuckle, J. C. Patton, M. H. Cosh, V. A. Walker, B. D. Carr, and S. D. Logsdon, 2015: Different rates of soil drying after rainfall are observed by the SMOS satellite and the South Fork in situ soil moisture network. *J. Hydrometeor.*, **16**, 889–903, https://doi.org/10.1175/JHM-D-14-0137.1.

Rong, Y., P. Bates, and J. Neal, 2022: Quantifying the impact of soil moisture dynamics on UK flood hazard under climate change. *24th EGU General Assembly*, Vienna, Austria, European Geosciences Union, EGU22-3213, https://doi.org/10.5194/egusphere-egu22-3213.

Rowland, C. S., R. D. Morton, L. Carrasco, G. McShane, A. W. O'Neil, and C. M. Wood, 2017: Land Cover Map 2015 (1km dominant aggregate class, GB). NERC Environmental Information Data Centre, accessed 31 January 2023, https://doi.org/10.5285/711c8dc1-0f4e-42ad-a703-8b5d19c92247.

Ruscica, R. C., J. Polcher, M. M. Salvia, A. A. Sörensson, M. Piles, E. G. Jobbágy, and H. Karszenbaum, 2020: Spatio-temporal soil drying in southeastern South America: The importance of effective sampling frequency and observational errors on drydown time scale estimates. *Int. J. Remote Sens.*, **41**, 7958–7992, https://doi.org/10.1080/01431161.2020.1767825.

Schwingshackl, C., M. Hirschi, and S. I. Seneviratne, 2017: Quantifying spatiotemporal variations of soil moisture control on surface energy balance and near-surface air temperature. *J. Climate*, **30**, 7105–7124, https://doi.org/10.1175/JCLI-D-16-0727.1.

Sehgal, V., N. Gaur, and B. P. Mohanty, 2021a: Global surface soil moisture drydown patterns. *Water Resour. Res.*, **57**, e2020WR027588, https://doi.org/10.1029/2020WR027588.

——, ——, and ——, 2021b: Global flash drought monitoring using surface soil moisture. *Water Resour. Res.*, **57**, e2021WR029901, https://doi.org/10.1029/2021WR029901.

Seneviratne, S. I., T. Corti, E. L. Davin, M. Hirschi, E. B. Jaeger, I. Lehner, B. Orlowsky, and A. J. Teuling, 2010: Investigating soil moisture–climate interactions in a changing climate: A review. *Earth-Sci. Rev.*, **99**, 125–161, https://doi.org/10.1016/j.earscirev.2010.02.004.

Shellito, P. J., and Coauthors, 2016: SMAP soil moisture drying more rapid than observed in situ following rainfall events. *Geophys. Res. Lett.*, **43**, 8068–8075, https://doi.org/10.1002/2016GL069946.

——, E. E. Small, and B. Livneh, 2018: Controls on surface soil drying rates observed by SMAP and simulated by the Noah land surface model. *Hydrol. Earth Syst. Sci.*, **22**, 1649–1663, https://doi.org/10.5194/hess-22-1649-2018.

Stanley, S., and Coauthors, 2021: Daily and sub-daily hydrometeorological and soil data (2013–2019) [COSMOS-UK]. NERC Environmental Information Data Centre, accessed 31 January 2023, https://doi.org/10.5285/b5c190e4-e35d-40ea-8fbe-598da03a1185.

Talebi, A., R. Uijlenhoet, and P. A. Troch, 2007: Soil moisture storage and hillslope stability. *Nat. Hazards Earth Syst. Sci.*, **7**, 523–534, https://doi.org/10.5194/nhess-7-523-2007.

Tanguy, M., H. Dixon, I. Prosdocimi, D. G. Morris, and V. D. J. Keller, 2021: Gridded estimates of daily and monthly areal rainfall for the United Kingdom (1890–2019) [CEH-GEAR]. NERC EDS Environmental Information Data Centre, accessed 31 January 2023, https://doi.org/10.5285/dbf13dd5-90cd-457a-a986-f2f9dd97e93c.

——, and Coauthors, 2022: Soil moisture product merged from satellite and modelled data for Great Britain, April 2015-December 2017. NERC EDS Environmental Information Data Centre, accessed 31 January 2023, https://doi.org/10.5285/26b8ddd4-09fd-4e40-a556-6a8f3a7481ea.

Teuling, A. J., S. I. Seneviratne, C. Williams, and P. A. Troch, 2006: Observed timescales of evapotranspiration response to soil moisture. *Geophys. Res. Lett.*, **33**, L23403, https://doi.org/10.1029/2006GL028178.

Tomer, S. K., A. Al Bitar, M. Sekhar, M. Zribi, S. Bandyopadhyay, and Y. Kerr, 2016: MAPSM: A spatio-temporal algorithm for merging soil moisture from active and passive microwave remote sensing. *Remote Sens.*, **8**, 990, https://doi.org/10.3390/rs8120990.

Troch, P. A., T. Lahmers, A. Meira, R. Mukherjee, J. W. Pedersen, T. Roy, and R. Valdés-Pineda, 2015: Catchment coevolution: A useful framework for improving predictions of hydrological change? *Water Resour. Res.*, **51**, 4903–4922, https://doi.org/10.1002/2015WR017032.

Tso, C.-H. M., O. Kuras, and A. Binley, 2019: On the field estimation of moisture content using electrical geophysics: The impact of petrophysical model uncertainty. *Water Resour. Res.*, **55**, 7196–7211, https://doi.org/10.1029/2019WR024964.

Turner, S., L. J. Barker, J. Hannaford, K. Muchan, S. Parry, and C. Sefton, 2021: The 2018/2019 drought in the UK: A hydrological appraisal. *Weather*, **76**, 248–253, https://doi.org/10.1002/wea.4003.

Vergopolan, N., N. W. Chaney, H. E. Beck, M. Pan, J. Sheffield, S. Chan, and E. F. Wood, 2020: Combining hyper-resolution land surface modeling with SMAP brightness temperatures to obtain 30-m soil moisture estimates. *Remote Sens. Environ.*, **242**, 111740, https://doi.org/10.1016/j.rse.2020.111740.

——, and Coauthors, 2021: SMAP-HydroBlocks, a 30-m satellite-based soil moisture dataset for the conterminous US. *Sci. Data*, **8**, 264, https://doi.org/10.1038/s41597-021-01050-2.

——, and Coauthors, 2022: High-resolution soil moisture data reveal complex multi-scale spatial variability across the United States. *Geophys. Res. Lett.*, **49**, e2022GL098586, https://doi.org/10.1029/2022GL098586.

Wagner, W., and Coauthors, 2013: The ASCAT soil moisture product: A review of its specifications, validation results, and emerging applications. *Meteor. Z.*, **22**, 5–33, https://doi.org/10.1127/0941-2948/2013/0399.

Wang, Y., J. Mao, M. Jin, F. M. Hoffman, X. Shi, S. D. Wullschleger, and Y. Dai, 2021: Development of observation-based global multilayer soil moisture products for 1970 to 2016. *Earth Syst. Sci. Data*, **13**, 4385–4405, https://doi.org/10.5194/essd-13-4385-2021.

Wasko, C., R. Nathan, L. Stein, and D. O'Shea, 2022: Historical increases in flood variability due to changing storm volumes and soil moisture. *24th EGU General Assembly*, Vienna, Austria, European Geosciences Union, EGU22-128, https://doi.org/10.5194/egusphere-egu22-128.

Zha, Y., J. Yang, J. Zeng, C.-H. M. Tso, W. Zeng, and L. Shi, 2019: Review of numerical solution of Richardson–Richards equation for variably saturated flow in soils. *WIREs Water*, **6**, e1364, https://doi.org/10.1002/wat2.1364.

Zhou, S., and Coauthors, 2019: Land–atmosphere feedbacks exacerbate concurrent soil drought and atmospheric aridity. *Proc. Natl. Acad. Sci. USA*, **116**, 18 848–18 853, https://doi.org/10.1073/pnas.1904955116.

Zreda, M., D. Desilets, T. P. A. Ferré, and R. L. Scott, 2008: Measuring soil moisture content non-invasively at intermediate spatial scale using cosmic-ray neutrons. *Geophys. Res. Lett.*, **35**, L21402, https://doi.org/10.1029/2008GL035655.

——, W. J. Shuttleworth, X. Zeng, C. Zweck, D. Desilets, T. Franz, and R. Rosolem, 2012: COSMOS: The COsmic-ray soil moisture observing system. *Hydrol. Earth Syst. Sci.*, **16**, 4079–4099, https://doi.org/10.5194/hess-16-4079-2012.